

# Present-day mass loss rates are a precursor for West Antarctic Ice Sheet collapse

Tim van den Akker<sup>1</sup>, William H. Lipscomb<sup>2</sup>, Gunter R. Leguy<sup>2</sup>, Jorjo Bernales<sup>3</sup>, Constantijn J.

5 Berends<sup>1</sup>, Willem Jan van de Berg<sup>1</sup>, Roderik S.W. van de Wal<sup>1,4</sup>

<sup>1</sup>Institute for Marine and Atmospheric Research Utrecht, Utrecht University, Netherlands

<sup>2</sup>Climate and Global Dynamics Laboratory, NSF National Center for Atmospheric Research, Boulder, CO, USA

<sup>3</sup>Danish Meteorological Institute, Copenhagen, Denmark

<sup>4</sup>Department of Physical Geography, Utrecht University, Netherlands

10 *Correspondence to:* Tim van den Akker (t.vandenakker@uu.nl)

**Abstract.** Observations of recent mass loss rates of the West Antarctic Ice Sheet (WAIS) raise concerns about its stability since a collapse would increase global sea levels by several meters. Future projections of these mass loss trends are often estimated using numerical ice sheet models. However, **several** current models display low skill in reproducing **present-day**, observed mass change rates **at local scales**. Here, we **present an improved** initialization method that optimizes **local** agreement not only with observations of ice thickness and surface velocity, but also with satellite-based estimates of mass change rates. **This is achieved by a combination of tuned thermal forcing under the floating ice shelves and friction under the ice sheet.** Starting from this improved present-day state, we generate an ensemble of future **simulations** of Antarctic mass change **by varying** model **physics** choices **and** parameter values **while fixing the climate forcing at present-day values**. **The dynamical response shows** slow **grounding line** retreat over several centuries, followed by a **phase of rapid mass loss over about 200 years** **with a consistent rate of ~3 mm GMSL/yr**. We find that for all ensemble members, the Thwaites and Pine Island glaciers collapse. Our results imply that **present-day ocean thermal forcing, if held constant over multiple centuries, may be sufficient to deglacierate** large parts of the WAIS, **raising global mean sea level** by at least a meter.

## Introduction

25 The projected Antarctic contribution to global mean sea level (GMSL) rise ranges from 0.03 m (SSP1-1.9, low end of the likely range) to 0.34 m (SSP5-8.5, high end of the likely range) in 2100 (Fox-Kemper et al., 2021). **Dynamical** processes are not expected to **accelerate or decelerate ice mass change significantly** before 2100 (Van De Wal et al., 2022). **After 2100, however, dynamical processes are highly uncertain, possibly accelerating GMSL rise significantly** (Fox-Kemper et al., 2021; Payne et al., 2021).

Deleted: most

Deleted: accurately.

Deleted: develop a new

Deleted: projections

Deleted: , covering uncertainties in

Deleted: ,

Deleted: and (observational) input data. Our ensemble displays a

Deleted: speed-up that lasts around

Deleted: .

Deleted: , even though the climate is held constant at present-day values.

Deleted: today's mass loss rates are a precursor of the deglaciation of

Deleted: which would raise

Deleted: levels

Deleted: in the coming centuries, without additional climate forcing.

Deleted: 1

Formatted: Font: Bold

Formatted: Normal

Deleted: SSP8

Deleted: This range is reasonably constrained as dynamical

Formatted: Font: 12 pt, Ligatures: Standard + Contextual

Deleted: make a large contribution

Deleted: (van de Wal et al., 2022). After 2100, however, dynamical processes are highly uncertain, possibly raising GMSL by multiple meters before 2300

Deleted: ,

55 ~~One such process is the Marine Ice Sheet Instability (MISI; see Schoof (2012, 2007) and Durand et al. (2009), which could drive a mostly dynamical irreversible retreat (i.e., the recovery time is substantially longer than the response time) of marine-terminating glaciers. Robel et al. (2019) argued that the mere possibility of MISI amplifies uncertainty in sea level rise projections from ice sheet models. MISI can occur for parts of the ice sheet where outlet glaciers terminate on a retrograde-sloping, submerged bedrock, due to a positive feedback between the flux across the grounding line (GL, the transition line~~  
60 ~~between a grounded ice sheet and a floating ice shelf) and the ice thickness at the GL. Thwaites Glacier (TG) and Pine Island Glacier (PIG), in the Amundsen Sea region of the West Antarctic Ice Sheet (WAIS), are located in such regions and may therefore be vulnerable to MISI.~~

Currently, the Thwaites GL retreats by up to 1.2 km per year on the eastern shelf and up to 0.9 km per year along the western margin (Milillo et al., 2019), and the GL of PIG retreated 31 km in 20 years (Rignot et al., 2014). Warm Circumpolar Deep  
65 Water (CDW) and related ~~high~~ basal melt rates have been observed under Pine Island Glacier (Jacobs et al., 2011a) since the early 1990s, and model studies show that CDW intrusions have coincided with PIG speedup (Thoma et al., 2008; Jenkins et al., 2016). As a result, the Amundsen Sea Embayment (ASE, which contains TG and PIG) is currently the largest contributor to Antarctic Ice Sheet (AIS) mass loss (Smith et al., 2020; Rignot et al., 2019). Further retreat of PIG and TG would increase ice drainage from these basins into the ocean, eventually triggering the collapse (i.e. relatively fast, potentially irreversible  
70 ungrounding and ice loss) of a significant part of the WAIS over several centuries.

Several modelling studies have assessed the potential for ASE collapse. One study (Joughin et al., 2014) argued that under present-day melt rates, TG might already be on a trajectory toward ~~accelerated~~ retreat; moderate retreat in this century will likely be followed by a phase of rapid collapse beginning in the next 200 to 900 years. Another study (Favier et al., 2014)  
75 used three ice sheet models to show that PIG is now undergoing a climate-driven 40-km retreat, but they made no projections on longer time scales. Both studies mention MISI as the main driver of retreat, but the retreat might be reversed by sufficient ocean cooling (Favier et al., 2014). Some subsequent studies suggest that TG and PIG are unstable under the current climate and could collapse on a timescale up to 2000 years (Golledge et al., 2021; Coulon et al., 2024), while others  
80 suggest that the two glaciers will require additional forcing to collapse (Feldmann and Levermann, 2015; Arthern and Williams, 2017; Reese et al., 2023; Garbe et al., 2020). Lipscomb et al. (2021) projected accelerated retreat leading to a collapse only when ocean thermal forcing increases by 1–2 K relative to a preindustrial or 20th century equilibrium. However, there are few historical observations of Southern Ocean temperatures, so it is unknown how much the ASE has warmed in the past century, and if the warming needed to drive such a retreat has already happened. It is therefore unknown whether ASE glacier retreat will persist and eventually accelerate under present-day climate conditions.

85 Studying ASE glacier stability requires century-scale model simulations, which contain significant uncertainties. Seroussi et al. (2024) found that potential AIS contributions to GMSL rise dramatically after 2100, with large variations across ice sheet

**Deleted:** One uncertain process is the Marine Ice Sheet Instability (MISI; Pattyn et al. (2018)), which could drive the unforced irreversible retreat of marine-terminating glaciers. MISI might occur for parts of the ice sheet where unbuttressed outlet glaciers terminate on a retrograde-sloping, submerged bedrock, due to a positive feedback between the flux across the grounding line (GL, the transition line between a grounded ice sheet and a floating ice shelf) and the ice thickness at the GL. Thwaites Glacier (TG) and Pine Island Glacier (PIG), in the Amundsen Sea region of the West Antarctic Ice Sheet (WAIS), are in such locations and may be (... [1])

**Deleted:** higher

**Deleted:** (Jacobs et al., 2011) since the early 1990s, and rest (... [2])

**Deleted:** (Thoma et al., 2008, Jenkins et al., 2016).

**Deleted:** (Rignot et al., 2019, Smith et al., 2020).

**Deleted:** (Sun et al., 2020).

**Deleted:** under current climate forcing

**Formatted:** Font: 12 pt, Ligatures: Standard + Contextual

**Deleted:** irreversible

**Formatted:** Font: 12 pt, Ligatures: Standard + Contextual

**Deleted:** an unstable

**Deleted:** (

**Deleted:** makes

**Deleted:** after this). The

**Deleted:** could

**Deleted:** . Both studies mention MISI as the main driver of (... [3])

**Formatted:** Font: 12 pt, Ligatures: Standard + Contextual

**Deleted:** of a few centuries

**Deleted:** Joughin et al., 2014, Arthern and Williams, 2017,

**Deleted:** .

**Deleted:** 2023

**Deleted:** . In contrast, other studies have argued that under t (... [4])

**Formatted:** Font: 12 pt, Ligatures: Standard + Contextual

**Deleted:** .

**Formatted:** Font: 12 pt, Ligatures: Standard + Contextual

**Deleted:** . Garbe et al., 2020, Rosier et al., 2021,

**Deleted:** . For example, one study (Reese et al., 2023) ran a (... [5])

**Deleted:** (Garbe et al., 2020, Lipscomb et al., 2021). There

**Deleted:** not possible to conclude from those studies

**Deleted:** the

**Deleted:** in the WAIS

**Deleted:** sustain

**Deleted:**

**Deleted:** Studying ASE stability under current climate cond (... [6])

160 models. According to Aschwanden et al. (2021), uncertainties in ice sheet modelling arise from four main sources: suboptimal model initialization, incomplete understanding of physical processes, numerical model uncertainty, and uncertainty in the climate forcing. Some ice sheet models are initialized using a long spin-up to steady state. These models often struggle to represent the observed mass change of recent decades, because the result of a steady state initialization is a stable ice sheet without model drift. A good representation of recent mass changes is essential for reliable projections, as these changes are likely to continue or accelerate.

165 Broadly, two methods are used to initialize ice sheet models: data assimilation and spin-up. In the first, data assimilation methods (Larour et al., 2012; Gudmundsson et al., 2012; Cornford et al., 2015; Hoffman et al., 2018; Bradley and Arthern, 2021) capture conditions at a certain time. For example, based on the observed ice thickness, the ice surface velocities are calculated and compared to observations. Uncertain parameters are tuned to minimize a cost function based on the difference

170 between observed and modelled quantities until the velocities converge to a state close to observations. This has the advantage that the resulting ice sheet matches the observed thickness and is ideally close to observed velocities at the start of a forward run, without necessarily being in steady state. However, the resulting dynamic state might not replicate the observed mass change rates. The simulation of recent mass change can be improved where annual or subannual observations are available, by doing a transient calibration as suggested by Goldberg et al. (2015). Also, the modelled mass

175 change rates can be added to the cost function, as was done for example by Rosier et al. (2021) to minimize model drift. Alternatively, Bett et al. (2023) used the ice sheet model WAVI (Arthern et al., 2015) and added the difference between observed and modeled mass change rates to the cost function, using observed mass change rates from Smith et al. (2020). The WAVI inversion method yields spatially varying values of two free parameters relating to basal friction and ice

180 viscosity. Since both ice velocities and mass change rates are targeted simultaneously through the cost function, it is likely that there is a trade-off between errors in these quantities and that the modelled mass change rates do not agree with observations in all locations. Neither Arthern et al. (2015) nor Bett et al. (2023) give a quantitative comparison of modelled and observed mass change rates. More recently, Rosier et al. (2024) used the misfit between observed and modelled mass

185 change rates in their data assimilation inversion, similar to Rosier et al. (2021). They state explicitly that it is not possible to obtain a perfect fit for both ice surface velocities and observed mass change rates, since those two datasets are not mutually consistent.

The other initialization approach is the spin-up method (Winkelmann et al., 2011; Pollard and Deconto, 2012; Greve and Blatter, 2016; Quiquet et al., 2018; Lipscomb et al., 2019; Berends et al., 2021; Berends et al., 2022), which consists of a long (typically several thousands of years) run with paleoclimatic or preindustrial forcing during which the ice sheet can freely evolve. Optionally, uncertain parameter values can be tuned to nudge variables like ice thickness and surface

190 velocities toward present-day observed values. This happens in model runtime: at regular intervals, one or more free parameters are adjusted as necessary to decrease the misfit between the model and observations. The resulting ice sheet is

Deleted: (DA)

Deleted: 2012, Larour et al.,

Deleted: ,

Deleted: ,

Deleted: ,

**Deleted:** are used to iterate toward a specific state. For example, based on the observed ice thickness, the ice surface velocities are calculated and compared to observations. Uncertain parameters are tuned iteratively until the velocities converge to a state close to observations. This has the advantage that the resulting ice sheet matches the observed thickness and velocities at the start of a forward run, without being necessarily in steady state. However, the model drift, when run forward, can be erratic if ice thickness and surface velocity observations are not mutually consistent. Subsequently, where physically realistic, the drift still does not necessarily equal the observed mass change rates, as, so far, matching the observed mass change is not used as optimisation target.¶

The other approach is the spin-up method (Winkelmann et al., 2011, Pollard and Deconto, 2012, Greve and Blatter, 2016, Quiquet et al., 2018, Lipscomb et al., 2019, Berends et al., 2021, Berends et al., 2022) consists of a run with paleoclimatic or preindustrial forcing during which the ice sheet can freely evolve. Uncertain parameter values can be tuned, to nudge variables like ice thickness and surface velocities toward present-day observed values. The resulting ice sheet is ideally close to observations and in near equilibrium with little drift. The modeled ice sheet can also be tuned to historical (e.g., 20th century) estimates or observations, and then advanced to the present-day using GCM forcing, to avoid an unrealistic steady state at the start of a forward run (Coulon et al., 2023, Reese et al., 2023). A further challenge in modeling the observed present-day mass change rates through the ice-sheet model initialization is that the magnitudes and spatial patterns of historical sub-shelf melt rates are poorly constrained by observations and models. Global climate models (GCMs) generally do not simulate large Amundsen Sea warming in the recent past (Naughten et al., 2022). Thus, forcing an ice sheet model with ocean output from GCMs will tend to underestimate current melt and thinning. ¶

We therefore developed an addition to the spin-up method. Our initialization procedure expands this method by equilibrating the modeled ice sheet to the mass balance corrected with the observed mass change rates at individual grid points, before starting future runs. The observed mass change rates are derived from satellite-observed surface elevation change rates

235 ideally close to observations and in near equilibrium with little drift (i.e., with little mass change). The modeled ice sheet can  
also be tuned to historical estimates or observations, and then advanced to the present-day using forcing from global climate  
models (GCMs), to avoid an unrealistic steady state at the start of a forward run (Reese et al., 2023; Coulon et al., 2024).  
This has the advantage of obtaining the modelled mass change rates through a physical process (ocean warming or changes  
in the surface mass balance), but this adds two uncertainties: the ice sheet geometry from before the observational period,  
240 along with the forcing over the historical period.

This study describes an addition to the spin-up method to match observed mass change rates at the start of forward  
simulations without relying on uncertain historical ice sheet geometry and forcing. This method is similar to the mass  
balance modification mentioned in Hill et al. (2023), but instead of minimizing mass change rates, we aim to match the  
observed rates. These rates are derived from satellite-observed surface elevation changes (Smith et al., 2020), corrected for  
245 firm processes and glacial isostasy. We apply this method to the Community Ice Sheet Model (CISM, Lipscomb et al. (2021);  
Lipscomb et al. (2019), allowing us to initialize the Antarctic Ice Sheet in its observed disequilibrium. We use this setup to  
conduct forward simulations without changing the climate forcing. In these simulations, we find that Thwaites Glacier, Pine  
Island Glacier and eventually large parts of the WAIS collapse over many centuries. We run similar simulations using the  
Utrecht Finite volume Ice Sheet Model UFEMISM (Berends et al., 2021), to show that the method can be easily  
250 implemented across models and to make sure that WAIS collapse is not unique to CISM.

Section 2 describes the two ice sheet models, the initialization method, and the subsequent forward runs. In Sect. 3, we show  
that the new initialization procedure results in a modeled present-day state in CISM which is in very good agreement with  
observations (ice thickness RMSE 34 m, ice surface velocity RMSE = 121.2 m/yr, GL position on average within 1.5 km  
from the observed GL), and importantly has the same disequilibrium as observed by Smith et al. (2020). In Sect. 4, we  
255 discuss the default forward run, starting from the initialized state, under sustained present-day atmosphere and (inverted)  
ocean forcing, purposely excluding further climate forcing. We repeat the default simulation with UFEMISM (Sect. 5) to  
show that the observed retreat of TG and PIG is consistent in the two models. In Sect. 6, we show that the CISM behavior is  
robust under a wide variety of physical approximations and parameter settings. The manuscript ends with a discussion in  
Sect. 7 and a conclusion in Sect. 8.

## 260 2 Methods

### 2.1 CISM

The Community Ice Sheet Model (CISM; (Lipscomb et al., 2021; Lipscomb et al., 2019) is a thermo-mechanical higher-order  
ice sheet model, which is part of the Community Earth System Model version 2 (CESM2, Danabasoglu et al. (2020)). This  
study primarily uses CISM v2.1 and builds on earlier applications of CISM to Antarctic Ice Sheet retreat (Lipscomb et al.,

**Deleted:** This procedure avoids the potential DA biases, reduces the uncertainty associated with direct GCM forcing, and circumvents the need to represent the AIS in its unknown pre-industrial state.

**Deleted:** 2019),

**Deleted:** 2021

**Deleted:** ) at 4 km horizontal resolution, and the Utrecht Finite volume ice sheet model

**Deleted:** . These

**Deleted:** are described in detail in Section 2.

**Deleted:** Section

**Deleted:** demonstrate

**Deleted:** by

**Deleted:** 1.5 km from the observed GL), and importantly has the same disequilibrium as observed. In Section 4 we discuss the default forward run, starting from this

**Deleted:** Furthermore, we test an extensive variety of physical approximations and parameter settings in CISM and

**Deleted:** and will eventually accelerate even

**Deleted:** current climate conditions (Section 5). This

**Deleted:** conclusions

**Deleted:** Section 6

**Deleted:** (Lipscomb et al., 2019, Lipscomb et al., 2021))

**Deleted:** ).

**Deleted:** (Lipscomb et al., 2021, Berdahl et al., 2023).

290 [2021; Berdahl et al., 2023](#)). CISM is run at 4 km resolution with a vertically integrated higher-order approximation to the  
momentum balance ([Goldberg, 2011; Robinson et al., 2022](#)), with a regularized Coulomb sliding law (Zoet and Iverson, 2020)  
as basal boundary condition. We apply a surface mass balance and surface air temperature climatology spanning 1979-2016  
from RACMO version 2.3p2 (Van Wessem et al., 2018). Basal melt rates are calculated using a quadratic relation with a  
thermal forcing observational dataset (Jourdain et al., 2020). Internal ice temperatures are allowed to evolve freely during the  
initialization and the forward runs. Variable names and parameter values used in the following text are summarized in Tables  
295 1 and 2.

**Deleted:** (Goldberg, 2011, Robinson et al., 2022)

**Deleted:** the present-day

**Deleted:** UFEMISM v1.0 (Berends et al., 2021) is used to test whether the results depend on the numerical features of a single model....

Table 1. Variables used in this study.

Variables	Definition
$b$	Bedrock height, positive above sea level
$\dot{m}_{mta}$	Basal melt rates under floating ice
$C_c$	Basal friction coefficient (Coulomb $C_c$ ), inverted quantity in this study
$C_r$	Basal friction relaxation target
$H$	Modeled ice thickness
$H_f$	Ice thickness above floatation
$H_{obs}$	Observed ice thickness
$N$	Effective pressure
$TF_{base}$	Thermal forcing applied at the ice shelf draft
$u_b$	Basal ice speed
$\delta T$	Ocean temperature correction, inverted quantity in this study
$\tau_b$	Basal shear stress

**Deleted:**  $b_{mt}$

**Formatted:** Font: 12 pt

**Deleted:** )

**Deleted:** Thermal forcing from Jourdain et al. (2020) applied at the ice shelf draft

**Deleted:** velocities magnitude

Table 2. Parameters and their units and values used in this study.

Parameters	Values	Units	Definition
$c_{pw}$	3974	$J kg^{-1} K^{-1}$	Specific heat of seawater
$g$	9.81	$m s^{-2}$	Gravitational acceleration
$H_0$	100	m	Ice thickness scale in the inversion
$L_f$	$3.34 * 10^5$	$J kg^{-1}$	Latent heat of fusion
$m$	3	-	Basal friction exponent

**Deleted:** ¶

¶

**Deleted:** Definition

$T_r$	0	K	Relaxation target of the ocean temperature inversion
$u_0$	200	m yr <sup>-1</sup>	Yield velocity <a href="#">in the basal sliding law</a>
$p$	0.5	-	Exponent in effective pressure relation
$r$	<a href="#">0.05</a>	-	Strength of inversion relaxation
$\rho_i$	917	kg m <sup>-3</sup>	Density of ice
$\rho_w$	1027	kg m <sup>-3</sup>	Density of ocean water
$\tau$	100	yr	Time scale in the <a href="#">friction</a> inversion
$\gamma_0$	30000	m yr <sup>-1</sup>	Basal melt rate coefficient
$\tau_o$	<a href="#">25</a>	<a href="#">yr</a>	<a href="#">Time scale in the ocean temperature inversion</a>

Deleted: 5

Formatted Table

### 2.1.1 Basal friction

315 In the default configuration, basal friction is parameterized using a basal sliding law based on laboratory experiments (Zoet and Iverson, 2020). This sliding law combines elements of ice sliding on a hard bed (e.g., bedrock) with sliding on deformable soft beds (e.g., saturated till). Its end cases are Weertman-style sliding, with basal velocities dependent on some power of the basal friction, and Coulomb sliding, with basal friction and velocities decoupled. The former mechanism usually dominates where the ice sheet is [flowing on hard, non-deformable beds](#), while the latter describes fast-flowing outlet glaciers [with softer deformable till](#) such as Pine Island and Thwaites Glaciers. In CISM, the basal sliding law is implemented as follows:

Deleted: frozen to the bed

$$\tau_b = C_c N \left( \frac{u_b}{u_b + u_0} \right)^{\frac{1}{m}} \quad (1.1)$$

where  $C_c$  is a unitless parameter controlling the strength of the Coulomb sliding. In CISM,  $C_c$  corresponds to  $\tan \phi$  of Zoet and Iverson (2020), in which  $\phi$  is the friction angle, a material property of the subglacial till. Since  $C_c$  is poorly constrained by theory and observations, we use it as a spatially variable tuning parameter, which we tune in the following way using a nudging method (Lipscomb et al., 2021):

Deleted: ,

$$\frac{dC_c}{dt} = -C_c \left[ \left( \frac{H - H_{obs}}{H_0 \tau} \right) + \frac{2}{H_0} \frac{dH}{dt} + \frac{r}{\tau} \ln \frac{C_c}{C_r} \right] \quad (1.2)$$

Deleted:  $\left[ \left( \frac{H - H_{obs}}{H_0 \tau} \right) + \frac{2}{H_0} \frac{dH}{dt} + \frac{r}{\tau} \ln \frac{C_c}{C_r} \right]$

in which  $H$  is the modeled ice thickness,  $H_{obs}$  the observed ice thickness, and  $C_r$  the relaxation target for  $C_c$ .  $H_0$ ,  $\tau$  and  $r$  are empirical constants used to vary the [relative magnitude](#) of each term. The [third term in brackets, which is not included in Lipscomb et al. \(2021\), provides a relaxation target  \$C\_r\$ , that helps prevent  \$C\_c\$  from drifting toward extreme values \(limited to  \$10^{-6}\$  and 1\)](#). It is based on elevation, with lower values at low elevation where soft marine sediments are likely more prevalent.

Deleted: size

Deleted: is a 2D field

Deleted: inhibits very high and low

Deleted: of  $C_c$ .

Formatted: Subscript

340 We chose targets of 0.1 for bedrock below -700 m asl and 0.4 for above 700 m asl, with linear interpolation in between, similar to Aschwanden et al. (2013). Our values for  $H_0$  and  $\tau$  are respectively 100 m and 100 yr.

Deleted: linearly

Deleted: .

The effective pressure  $N$  in Eq. (1.1) is the pressure at the ice–bed interface, equal to the difference between the ice overburden pressure and the subglacial water pressure. The effective pressure is lowered near GLs to represent the connection of the subglacial hydrological system to the ocean (Leguy et al., 2014):

$$N = \rho_i g H \left(1 - \frac{H_f}{H}\right)^p \quad (1.3)$$

where  $\rho_i$  is the density of ice,  $g$  is gravitational acceleration,  $H$  is the ice thickness, and  $p$  is an exponent between 0 and 1, with a larger value implying a stronger ocean connection. A value of  $p=0.5$  is chosen in this study unless stated otherwise, to include some hydrological connection (Leguy et al., 2021; Lipscomb et al., 2021). Different values are tested in the sensitivity analysis. The flotation thickness  $H_f$  is the height of an ice column resting on bedrock below sea level ( $b < 0$ ) at hydrostatic equilibrium:

Deleted: (with a larger value implying a stronger ocean connection). The flotation thickness  $H_f$  is the height of an ice column resting on bedrock below sea level ( $b < 0$ ) at hydrostatic equilibrium; it is given by

$$H_f = \max\left(0, -\frac{\rho_w}{\rho_i} b\right) \quad (1.4)$$

where  $\rho_w$  is the density of sea water and  $b$  is the bedrock elevation.

Deleted: Runs in this study were done with  $p = 0.5$  unless stated otherwise.

### 2.1.2 Basal melt rates

355 Beneath grounded ice, CISM computes basal melt rates based on the net of geothermal, frictional, and conductive heat fluxes at the bed. In our runs, however, there is no coupling between basal water and sliding parameters. Beneath floating ice, we use the ISMIP6 local parameterization (Jourdain et al., 2020):

$$b_{melt} = \gamma_0 \left(\frac{\rho_w c_{pw}}{\rho_i L_f}\right)^2 (\max[TF_{base} + \delta T, 0])^2 \quad (1.5)$$

Deleted:  $b_{melt} = \gamma_0 \left(\frac{\rho_w c_{pw}}{\rho_i L_f}\right)^2$

The max function ensures non-negative melt rates; negative rates imply refreezing (accretion), which is not represented. We tune  $\delta T$  to optimize the ice thickness agreement with observations, similar to Eq. (1.2):

Deleted: like

360

$$\frac{d(\delta T)}{dt} = -\delta T \left[ \left(\frac{H - H_{obs}}{H_0 \tau_0}\right) + \frac{2}{H_0} \frac{dH}{dt} \right] + \frac{(T_r - \delta T)}{\tau_0} \quad (1.6)$$

Deleted:  $\frac{d(\delta T)}{dt} = -\delta T \left[ \left(\frac{H - H_{obs}}{H_0 \tau_0}\right) + \frac{2}{H_0} \frac{dH}{dt} \right] + \frac{(T_r - \delta T)}{\tau_0}$

where  $T_r$  is a relaxation target for the temperature correction. Ideally, the correction is small, and therefore we set  $T_r = 0$  everywhere. Melt rates are sensitive to  $\gamma_0$  in Eq. (1.5). We chose a default value  $\gamma_0 = 3.0 \times 10^4$  m/yr, for which the average  $\delta T$  in the TG and PIG basins at the end of the transient spin-up is close to 0. In other words, we assumed that the observed

Deleted:  $\uparrow$  where  $T_r$  is a relaxation target for the temperature correction. Ideally, the correction is small, and therefore we set  $T_r = 0$  everywhere. Melt rates are sensitive to  $\gamma_0$ . We chose a default value  $\gamma_0 = 3.0 \times 10^4$  m/yr, for which the average  $\delta T$  in the Thwaites basin at the end of the transient spin-up is close to 0. In other words, we assumed that the observed ocean temperatures in this region are of the right magnitude to drive basal melt rates consistent with observations.  $\uparrow$

ocean temperatures in this region are of the right magnitude to drive basal melt rates consistent with observations. Our value for  $\gamma_0$  lies about halfway between the median “MeanAnt” and “PIGL” calibration values suggested by Jourdain et al. (2020). The depth dependency is introduced in the dataset  $TF_{\text{base}}$  from Jourdain et al. (2020) in two ways. First, the thermal forcing increases with depth due to the decrease of the pressure melting point. Second, in the dataset of Jourdain et al. (2020), there is warm CDW present in the ASE with increasing thermal forcing with depth. In a forward run, we keep  $\delta T$  constant at the value computed during the spin-up. When the grounding line retreats, we extrapolate basin-average values of  $\delta T$  (basins are defined following Zwally et al. (2015)), to newly floating cells.

### 2.1.3 Grounding line subgrid-scale parameterization

The GL is not explicitly modeled in CISM but follows from the hydrostatic balance. The modeled GL cuts through cells, with some cells partly grounded and partly floating. To prevent abrupt jumps in modeled quantities at the GL, we use a GL parameterization (Leguy et al., 2021). We define a flotation function,

$$f_{\text{float}} = -b - \frac{\rho_i}{\rho_w} H \quad (1.7)$$

which varies smoothly from negative for grounded ice to positive for floating ice. (For floating ice,  $f_{\text{float}}$  is the thickness of the ocean cavity.)  $f_{\text{float}}$  is used to compute the floating fraction as a percentage of grid cell area by bilinearly interpolating its value from cell vertices to the cell areas scaled to the cavity thickness (Leguy et al. (2021)). The grounded and floating fraction of a cell are then used to scale basal friction and basal melting. For the basal melting, this is referred to as the Partial Melt Parameterization (PMP). Other parameterizations tested in the sensitivity experiments of this study are the Floatation Condition Melt Parameterization (FCMP), in which full melt is assigned to a cell once the cell center is floating, and the No Melt Parameterization (NMP), in which no melting is allowed in any cell that is partly grounded.

### 2.1.4 Calving

There are several calving laws in the literature (e.g., (Yu et al., 2019); Wilner et al. (2023); Greene et al. (2022)). However, there is no agreed-upon best approach to Antarctic calving (this holds for the Greenland Ice Sheet as well; see for example Benn et al. (2017)), and most calving laws struggle to reproduce the observed calving front at multiple locations simultaneously without adjusting local parameters (Amaral et al., 2020). We therefore choose to apply a no-advance calving scheme, preventing the calving front from advancing beyond the observed present-day location. The calving front can retreat, but only when it thins below a threshold thickness of 1 m. In most places, it does not move. This is a conservative approach for a retreating system; in practice, we would expect the calving front to move inland and therefore provide less buttressing for upstream ice. By taking a conservative approach, we rule out the possibility that a simplistic calving algorithm is (partly) responsible for the modelled retreat.

**Deleted:** Thus, the

**Deleted:** ).

**Deleted:** .

**Deleted:** , including applications to Antarctic ice shelves

**Deleted:** .

**Deleted:** ), Greene et al. (2022),

**Deleted:** ).

**Deleted:** .

**Deleted:** Since we are unable to attain an accurate initial state with a physically-based calving law, we err on the conservative side by applying a

**Deleted:** . With this scheme,

**Deleted:** cannot advance

**Deleted:** . It

**Deleted:** the calving front

**Moved down [1]:** ¶

2.

**Moved down [2]:** the Utrecht FinitE VoluMe Ice Sheet Model (UFEMISM) (Berends et al., 2021).

**Moved down [3]:** (Berends et al., 2021).

**Deleted:** than the model suggests.

**Deleted:** 2 UFEMISM ¶

We repeated the main experiment with

**Deleted:** We use the same initialization procedure, discussed in more detail later, and climate forcing as in the default CISM setup but apply a different momentum balance approximation and discretization scheme. ¶

¶

UFEMISM is a thermo-mechanical ice-sheet model designed for long-term simulations at targeted high resolution

**Deleted:** UFEMISM discretizes the hybrid SIA/SSA approximation to the stress balance (Bueler and Brown, 2009) and other physical equations on a dynamic adaptive triangular mesh. In this study, mesh resolution ranges from ~4 km at the grounding lines of PIG and TG, to ~60 km over slow-moving inland ice. Here we apply a Budd-type sliding law, see Eq 1.8

**Formatted:** Font: Not Bold

**Moved down [4]:** (sometimes referred to as a regularized Coulomb sliding law (Joughin et al., 2019)), which contains spatially-varying friction coefficients

**Moved down [5]:** Both calibrations are performed during model initialization, which brings the modeled ice sheet to a state of equilibrium with a prescribed set of boundary conditions. For this study, friction coefficients and ocean temperatures are inverted during the first 90,000 model years of the initialization, after which their values are kept fixed in time. The model is then run for another

**Deleted:** sub-shelf melt rates and the corresponding ocean temperatures needed to reproduce the target geometry over ice ... [7]



475 **2.2 Initialization methods**

Typically, CISM nudges basal friction parameters and ocean temperatures to optimize the agreement of ice thickness with observations, allowing a modest misfit (a misfit scale of  $H_0 = 100$  m in Eqs. (1.2) and (1.6)) to avoid overfitting, but without considering the observed mass change rates. We refer to this method as the ‘equilibrium spin-up. This results in a steady state, where the integrated SMB is in equilibrium with the integrated ice losses: the modeled calving and basal melt fluxes. There is no isostatic adjustment in the default experiments; we assume a static bedrock. The model converges within  $\sim 10^4$  model years, which is typically assessed by considering several criteria like change in ice mass ice area and ice velocities. A converged model state should not drift significantly when run forward with fixed inverted quantities. We calculate the model drift in the modelled ice sheet after stopping the inversion (i.e. by continuing the simulation with the inverted fields kept constant) for 2000 years. We accept an initialization as ‘stable’ once there is little to no instantaneous model drift and there is no TG and PIG collapse after 2000 years. Then, it is certain that a PIG and TG collapse is caused by applying present-day mass change rates, and not influenced by model drift.

The addition to the equilibrium spin-up, referred to as the transient spin-up, allows the model to reach a geometry in agreement with observations, similar to the result of the equilibrium initialization, while also allowing the ice to thin or thicken in agreement with satellite observations at the start of the forward run (i.e., at the present day). Our goal is to create the observed dynamic disequilibrium, so we want to include the observed mass change rates as a target. To hold the ice geometry near observed values during the spin-up, we apply a correction term equal to the negative of the observed mass change rates. That is, we artificially apply a thickening term to ice that is thinning and a thinning term to ice that is thickening. This procedure trains the model to produce mass change rates that are (nearly) identical to the observations during the subsequent forward run, when the correction term is removed.

The mass balances for respectively the equilibrium initialization and the transient spin-up, respectively, are given by

$$\frac{\delta H}{\delta t} = -\nabla F + B \quad (1.8)$$

$$\frac{\delta H}{\delta t} = -\nabla F + B + C \quad (1.9)$$

In these equations,  $\nabla F$  is the ice flux divergence,  $B$  the sum of the basal and surface mass balances, and  $C$  the correction term applied to hold the ice at the observed thickness during the spin-up. Ideally, the initialization procedure ends when the left-hand sides of Eqs. (1.8) and (1.9),  $\frac{\delta H}{\delta t}$ , are zero. Hence, at the end of the equilibrium initialization, which uses Eq. (1.8),  $\nabla F$  is being balanced by  $MB$ , and forward simulations start with  $\frac{\delta H}{\delta t} \approx 0$ . In Eq. (1.9), used for transient initialization, we end the

**Deleted:** 3

**Deleted:** We apply two initialization methods. The first method, the equilibrium initialization strategy,

**Deleted:** error (an error)

**Deleted:** This results in a steady state, where the integrated SMB is in equilibrium with the modeled calving and basal melt fluxes. This typically takes  $10^4$  model years.

**Formatted:** Font: Not Bold, Font colour: Accent 4, English (UK)

**Deleted:** second initialization procedure,

**Deleted:** both ice-flow models

**Deleted:** like

**Deleted:** at the present day). We start with the above-described procedure to achieve an ice-sheet configuration by nudging the ice thickness toward observations and while simultaneously calibrating basal friction coefficients under grounded ice and ocean temperatures below ice shelves.

**Deleted:** However, because the nudging procedure (by necessity) occurs over model time,

**Deleted:** will shift away from observations once

**Deleted:** are applied. We temporarily prevent

**Deleted:** from happening by re-supplying the lost ice in areas that are...

**Deleted:** removing the accumulated ice in areas that are thickening. If we set this “correction term” equal to minus the observed mass change rates, then by the time the nudging procedure has achieved a constant geometry, we will have trained

**Deleted:** ice fluxes

**Deleted:** reality.

**Deleted:** In our transient

**Deleted:** method

**Deleted:** therefore “train” the

**Formatted:** English (UK)

535 initialization when  $\frac{\delta H}{\delta t} \approx 0$ . When we remove the  $C$  term, forward simulations start with  $\frac{\delta H}{\delta t} \approx -C$ , where the right-hand side is equal to the observed mass change rate, as desired.

The inversion methods are stopped when the modelled ice sheet has little to no model drift once run forward with the inverted friction and ocean temperatures, and particularly no significant ice mass loss in the ASE basin. The modelled ice sheet should ideally have little instantaneous drift compared to the observed mass change rates, and no thinning or collapsing glaciers during a continuation run of 2000 years with fixed inverted quantities and no mass change rates applied.

540 During a 2000 years model drift experiment, the model tends to grow to a slightly advanced state for PIG and the Dotson ice shelf, see Fig S1, S2, and S3. This advance is mostly due to the local positive feedback between the ice shelf geometry and basal melt rates that amplifies any small residual drift. Model drift is largely reduced in a forward run with a time-constant instead of geometry based (e.g. Eq. 1.5) basal melt rate field (not shown). Initialization takes about  $10^4$  model years.

### 545 2.3 Forward simulations

Forward simulations are continued without additional climate forcing, to assess the impact of the present-day ocean thermal forcing on the evolution of the AIS, and thereby the sea-level contribution over time. The future simulation using the transient spin-up method is referred to from now on as the “default experiment”. As the thermal forcing at a given ocean depth does not change, the modeled future evolution of the ice sheet is the response to the present-day forcing.

555 In forward simulations, the ice sheet starts to retreat after the mass correction term in the spin-up is removed. This has implications for the inverted  $C_c$  and ocean temperatures in cells that change from grounded to floating or vice versa. If grid points initialized as grounded ice become afloat, we extrapolate the basin-average ocean temperature corrections under the shelf from the end of the initialization. If initially floating grid points become grounded, we use an elevation-dependent parameterization to estimate the local  $C_c$ , similar to what was done in Aschwanden et al. (2013) and the same as what was used to calculate the relaxation target  $C_{r, \dots}$ .

560 The default forward simulation is compared against an extensive set of sensitivity experiments with modified physics and parameter choices. We designed these experiments conservatively, with many model choices that would tend to stabilize the modelled ice sheet and could potentially stop PIG and TG from collapsing PIG. Section 6 and the supplementary material describe the sensitivity experiments.

### 565 2.4 UFEMISM

**Deleted:** to equilibrate toward a state

**Deleted:** which

**Deleted:** are implicitly accounted for. For ice shelves with rapid

**Deleted:** observed, the mass correction is

**Deleted:** , which allows ocean temperatures to remain warmer than without the correction. Similarly, where grounded ice is thinning, we apply a positive mass correction

**Deleted:** allows basal friction to be weaker than it would be otherwise...

**Deleted:** ¶  
The default experiment taking off from the transient initialization is compared against an extensive set of parameter and model choice experiments, to assess the effect of uncertain or crudely represented physical processes and parameter values. We designed the set of experiments conservatively; we mostly selected model choices that would make the ice sheet theoretically more stable. See Fig. 4, Table 3, and the Extended Data for a detailed description. ¶

**Deleted:** 8

**Deleted:** A forward simulation departing from the transient initialization method starts by stopping the inversion and simultaneously removing the correction term from the mass balance. As a result, the ice will start to thin/thicken at (almost) exactly the observed rates, with ideally only a very small model drift. These

**Deleted:** mass change rates

**Deleted:** (unforced)

**Deleted:** unforced

**Deleted:** this initialization strategy

**Deleted:** We stress that the future evolution

**Deleted:** include future climate forcing, so

**Deleted:** purely the result of

**Deleted:** imbalance. Complementary to these default experiments, we verified if model drift is negligible with forward runs in which the mass balance correction term remains included. These results show that the model drift is negligible (Fig. S6). On longer timescales (2 kyrs), the model tends to grow to a slightly advanced state for PIG and the Dotson ice shelf. These advances are mostly due to local positive feedback between the ice shelf geometry and basal melt rates, as these advances are largely reduced in a forward run with time-constant basal melt rates (not shown).

**Formatted:** Font: Not Bold, Font colour: Auto

**Moved (insertion) [1]**

**Formatted:** Font: Not Bold

We repeated the default experiment with the transient spin-up using the Utrecht Finite Volume Ice Sheet Model (UFEMISM) (Berends et al., 2021). We use the same transient initialization procedure including the mass change rates from Smith et al. (2020) in the mass balance equation, and climate forcing as in the default CISM experiment, but apply a different momentum balance approximation, basal friction law, calving algorithm, and discretization scheme.

UFEMISM is a thermo-mechanical ice-sheet model designed for long-term simulations at variable resolution, e.g. simultaneously high resolution at the grounding line and lower resolution in the slow-moving interior (Berends et al., 2021). In this study, UFEMISM discretizes the hybrid SIA/SSA approximation to the stress balance (Bueler and Brown, 2009) and other physical equations on a dynamic adaptive triangular mesh. Mesh resolution ranges from ~4 km at the grounding lines of PIG and TG, to ~60 km for slow-moving inland ice. We apply a Budd-type sliding law, see Eq. (1.10) (sometimes referred to as a regularized Coulomb sliding law (Joughin et al., 2019)), which contains spatially-varying friction coefficients that aim to represent subglacial substrate conditions:

$$\tau_b = \tau_a n(\phi) u_b^{\frac{1}{m}} N^q \quad (1.10)$$

We invert for  $\phi$  by nudging toward a target geometry (Bernales et al., 2017b; Pollard and Deconto, 2012). As part of this nudging method, UFEMISM simultaneously inverts for sub-shelf melt rates and the corresponding ocean temperatures needed to reproduce the target geometry over ice-shelf sectors (Bernales et al., 2017a). Both calibrations are performed during model initialization, which brings the modeled ice sheet to a state of equilibrium with a prescribed set of boundary conditions. For this study, friction coefficients and ocean temperatures are inverted during the first 90,000 model years of the initialization, after which their values are kept fixed in time. The model is then run for another 10,000 years, which allows it to evolve unperturbed until equilibrium is attained. From 100,000 years, the default experiment with the mass change rates is started. We use both the PMP (default) and FCMP subgrid-scale melting parameterizations from Leguy et al. (2021), as described above.

Moved (insertion) [2]

Moved (insertion) [3]

Moved (insertion) [4]

Moved (insertion) [5]

Moved down [6]: After the initialization phase,  $C_c$

Moved down [7]: There are several ways for the freshwater flux from a collapsing WAIS to influence the ocean properties of the Amundsen Sea and the Southern Ocean.

Moved down [8]: Since we use a standalone-ice sheet model in this study, and no consensus has been reached on the effect of the freshwater flux, we did not parameterize this effect. In future studies, freshwater feedbacks could be added by coupling the ice sheet model to a cavity-resolving ocean model.

Deleted: 2.5 Missing processes

We note two missing processes that could affect the ice evolution. First, the mass change rates on grounded ice are controlled by parameters in the basal sliding law.

Deleted: is kept constant during forward runs, not accounting for future evolution of the ice-bed interface (e.g., increased basal meltwater that could enhance sliding (Dow, 2019; Kazmierczak et al., 2024)). Possible feedbacks (see for example van der Wel et al. (2013), Rémy and Legresy (2004)) between the ice flow and the bed are only partly represented through the basal friction law and the calculation of the effective pressure on bedrock below sea level (which roughly represents a hydrological connection to the ocean).

Second, as ice shelves melt and retreat, adding freshwater to the ocean, there is no feedback on ocean temperature or salinity.

Deleted: For example, cooling of the Southern Ocean sea surface, warming of the deeper ocean layers, and reduced Antarctic Bottom Water formation (Swart et al., 2023). The freshwater input can directly influence the basal melt rates by stratifying the ocean just beyond the shelves, thus trapping heat in the subsurface ocean and ultimately increasing the heat transport into the cavities, resulting in higher basal melt rates (Flexas et al., 2022). An earlier study found a relation between freshwater flux and sea ice formation and the presence of warm and dense water in large AIS cavities: a freshwater flux stabilizes and stratifies the ocean flow in cavities, and prevents further warm water from flowing in (Hellmer, 2004). This is a negative feedback, in contrast to the study by Flexas et al. (2022). The exact effect of a large freshwater pulse into the ocean surrounding the AIS is unknown (Swart et al., 2023)

Deleted:

.....Page Break.....

### 3. Results: Transient present-day state

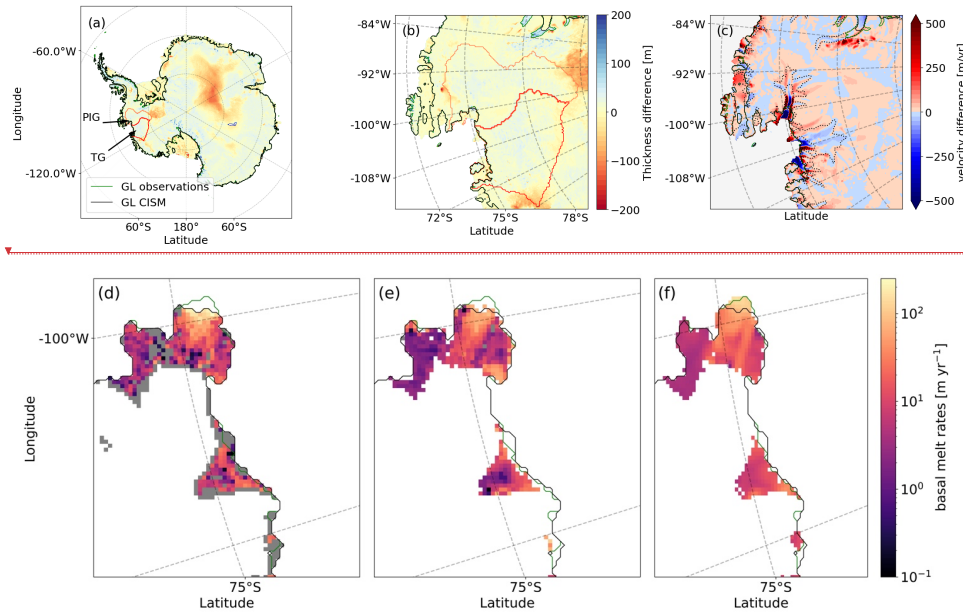
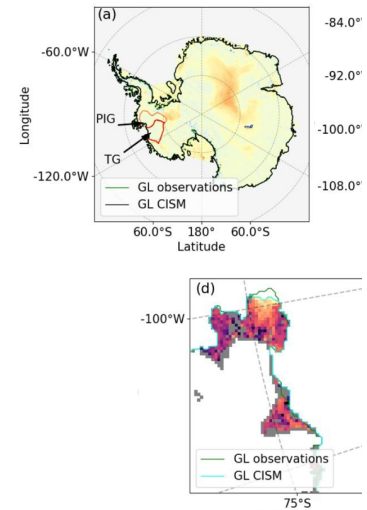


**Figure 1. Initialized state of the Antarctic Ice Sheet using CISM.** (Top row) Ice thickness difference between the final state of the transient initialization and observations for all of Antarctica (RMSE = 34 m, (a)) and the ASE region (RMSE = 19.3 m, (b)). The black line represents the modeled GL. The observed GL (green) is visible only where the modeled and observed GL deviate in position, for example at the PIG GL. Red and orange contours are drawn around the TG and PIG basins, respectively. (c) Surface ice velocity difference with respect to observations of Rignot et al. (2019). Positive differences indicate locations where CISM overestimates velocities. Observed surface velocities of 100 (outer) and 500 (inner) m/yr are contoured by black dots, to highlight fast-flowing regions with large velocities and gradients. For the ASE, the velocity RMSE = 99 m/yr. For ASE shelves only, the velocity RMSE = 216 m/yr. (Bottom row panel d,e,f) Basal melt rates, with grey and white denoting zero basal melt rates and no data, respectively, of (d) CISM with an integrated flux of 106 Gt/yr, (e) Adumilli et al. (2020) with an integrated flux of 94 Gt/yr, and (f) Rignot et al. (2013) with an integrated flux of 149 Gt/yr.

Figure 1 shows the modeled CISM state at the end of the transient initialization. The thickness error over the ASE region is low (RMSE = 19.3 m), and the GL closely follows observations, with an average 1.5 km difference (calculated as the average distance between the modeled GL position and the closest observed GL position). The modeled GL for PIG is shifted seaward



Deleted:

Formatted:

[8]

Deleted: entire

Deleted: Black contours represent

Formatted: Font: 9 pt

Formatted: Font: 9 pt

Deleted: Blue bars indicate the locations of the cross section

[9]

Formatted: Font: 9 pt

Deleted: Rignot et al. (2019)

Formatted: Font: 9 pt

Deleted: (

Deleted: is marked by grey cells, white cells contain

Deleted: )

Formatted: Font: 9 pt

Deleted: ((d),

Formatted: Font: 9 pt

Formatted

[10]

Formatted

[11]

Deleted: ((e),

Deleted: )

Deleted: ((f),

Deleted: ).

Formatted: Font: 9 pt

Formatted

[12]

Formatted: Font: 9 pt

Formatted: Font: 10 pt

Deleted: The resulting initialized state in UFEMISM is sh

[13]

by 5–10 km. The modeled basal melt rates and melt patterns beneath floating ice agree well with the values from Rignot et al. (2013) and Adusumilli et al. (2020), with an integrated melt flux within the range of the two datasets. The instantaneous and average model drift of this simulation is shown in Fig S1, S2 and the inverted quantities of both initializations are shown in S3. The initialized state in UFEMISM is shown in Fig. S4 and the inverted quantities in S5, and the result of the CISM equilibrium initialization in Fig. S6.

The modeled ice surface velocities are in good agreement with observations, even though they are not a target for assimilation. The RMSE of the ice surface velocities is comparable to other ISMIP6 models (Seroussi et al., 2020), of which the range is 100 – 400 m/yr. Many of those models are optimized to match observed velocities and use a variety of spin-up and data assimilation methods. Modeled PIG and Thwaites velocities are too low midstream and too high in the lateral margins, possibly because of the lack of brittle processes in CISM. These regions are heavily crevassed (Lhermitte et al., 2020); taking crevasses into account would weaken the ice, speed up the main flowlines, and slow down the margins, because the margins are then decoupled from the center flowline. The center flowline can accelerate and is not necessarily ‘dragging along’ the slower moving margins, which would bring our modelled ice surface velocities closer to observations. The integrated ice fluxes across the GLs of TG and PIG are close to the observations of Morlighem et al. (2020) (Fig. S7). As the integrated ice flux is in good agreement with observations, we believe that the dynamical characteristics of the model with a very accurate GL position and ice thickness and ice thickness changes almost equal to observations, are sufficient for our continuation experiments.

In the observations of Smith et al. (2020), the ASE shelves are thinning rapidly. Simulating these large negative mass change rates here requires higher ocean temperatures and lower basal friction under grounded ice compared to the equilibrium initialization. The greater friction during the equilibrium initialization leads to an underestimation of ice velocities (Fig S6). As a result, the grounding line flux is lower (see Fig. S7); therefore, lower basal melt rates and in general colder ocean conditions are required to match the observed ice shelf geometry.

The observed and modeled ice thickness change rates in the first years after the start of a default continuation run are shown in Fig. 2. The modelled mass change rate pattern over the first year (b) mimics the observations (a) in detail. After 5 years, the thinning rate of PIG decreases slightly, while the thinning rate of TG increases slightly.

Deleted: root mean square error (

Deleted: )

Deleted: , where many

Deleted: (Lhermitte et al., 2020)

Deleted: and

Deleted: . Since these

Deleted: compensating errors, the

Deleted: S1

Deleted: more important for the existence of the shelf than grid-cell-based velocities

Deleted: model’s dynamic

Deleted: (

Deleted: , good flux across the GL,

Deleted: )

Deleted: In the equilibrium initialization, ocean temperatures in the Amundsen Basin on average must be reduced by ~1 K compared to the thermal forcing dataset from Jourdain et al. (2020) to reproduce the observed ice shelf geometry. This is likely caused by an underestimation of modelled ice velocities in this region during the equilibrium initialization (Fig S3). As a result, the grounding line flux is lower (see Fig. S1), therefore, lower basal melt rates and in general colder ocean conditions are required to model the observed ice shelf geometry, compared to observations. Much smaller corrections of either sign are needed within the transient initialization method. This brings the basin average tuned ocean temperature perturbations closer to zero, highlighting that only a small correction on the ocean dataset is sufficient to produce the initialized state in equilibrium with the observed mass change rates using the ISMIP6 basal melt rate formulation, Eq. (1.5). Ignoring the observed mass changes rates in the initialization procedure results in a larger ocean temperature correction term. †

Deleted: S4

Deleted: modeled

Deleted: 5 years has broadly the same characteristics as

Deleted: . The

Deleted: , which is likely the result of

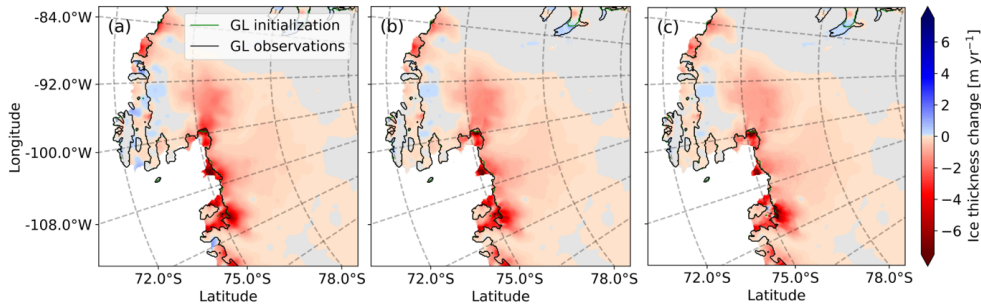


**Figure 2.** (a) Ice thickness change rates in the observations of Smith et al. (2020) with the observed grounding line in green and the modelled grounding line at the end of the transient initialization in green, in the ASE region. Modelled ice thickness change rates when starting a continuation run, from the transient initialization after 1 yr (b), and 5 yr (c).

#### 4. Results: Future state

In the default experiment with present-day climate forcing, AIS mass loss is dominated by the collapse of TG (including the neighboring Smith, Pope, and Kohler glaciers) and PIG (Fig. 3). In the first four centuries, mass loss is comparable to the current observed rates (Fig. 3b). During this period, the total AIS mass loss averages 0.5 mm GMSL yr<sup>-1</sup>, slightly less than the current combined loss from PIG and TG, because there is currently some East Antarctic Ice Sheet thickening, primarily in Dronning Maud Land (Smith et al., 2020), which continues in the forward simulation (Fig. 3a). Areas where little to no mass changes are observed in Smith et al. (2020), such as the Siple Coast and Victoria Land, remain in balance in our simulation.

After 500 years, the mass loss accelerates as both PIG and TG collapse. We can identify a shallow ridge in the TG bedrock profile approximately 45 km upstream of the present-day GL, which acts as the last pinning point before this accelerated collapse begins (see line AB in Fig. 3a and a zoom-in in Fig. 4). As soon as the grounding line passes over the line AB in Fig. 3a and Fig. 4, the high ridge approximately 45 km upstream of the present-day grounding line, the collapse starts. This second ridge at about 100 km upstream in the cross section CD of similar height as the ridge AB, but less extended in the cross-flow direction and surrounded by troughs, see Fig. 4.

**Deleted:** movement and buttressing. In fact, a pulse-like pattern is visible in the modeled mass change rates pattern in the first 50 years of ...

**Formatted:** Font: 9 pt, English (UK)

**Formatted:** Font: 9 pt, English (UK)

**Deleted:** , where thickening or thinning rates originate from grounding line changes and are subsequently advected in the direction of the calving front (see Supplementary Movie 1

**Formatted:** Font: 9 pt, English (UK)

**Deleted:** ¶  
¶

**Deleted:** continuation

**Deleted:** without further

**Deleted:** 2

**Deleted:** .

**Deleted:** effect of

**Deleted:** EAIS

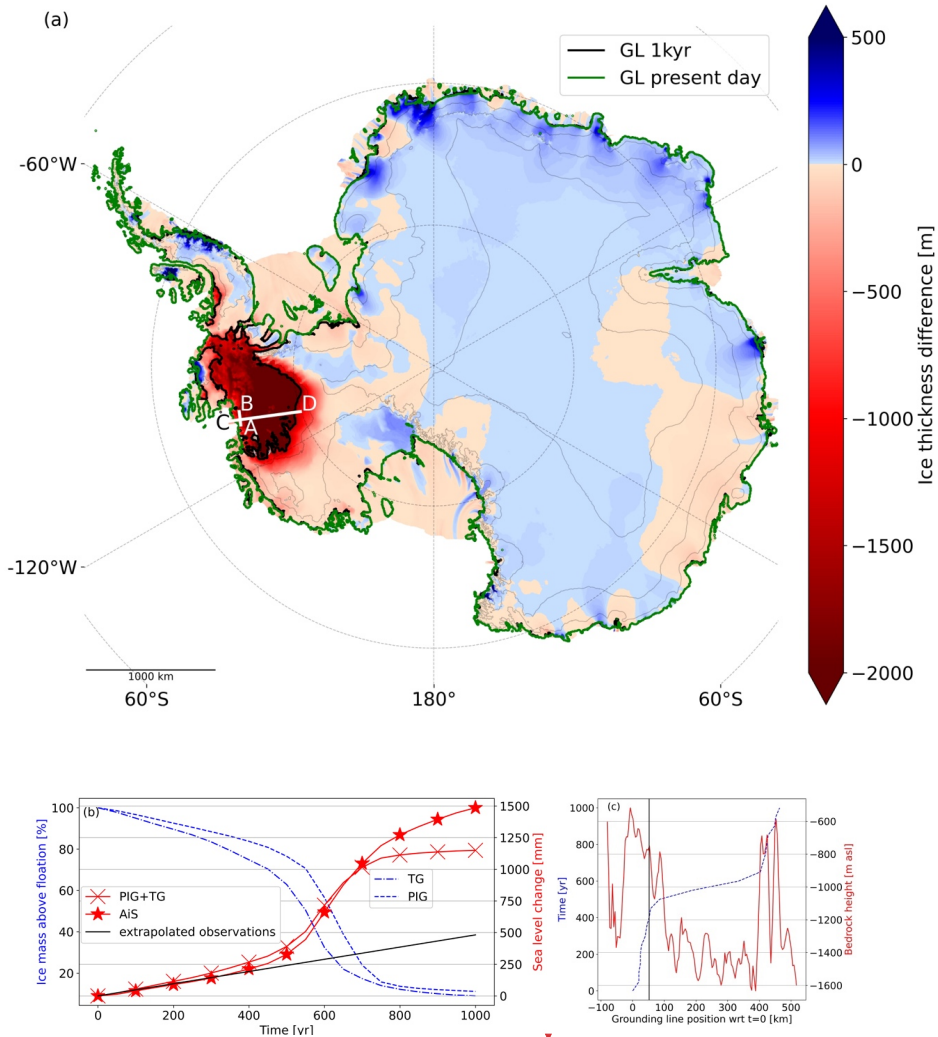
**Deleted:** persists

**Deleted:** continuation experiment (Fig. 2a). We can furthermore

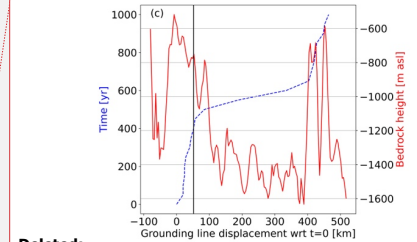
**Deleted:** the

**Deleted:** 2a and Extended Data Fig. S7).





850 **Figure 3. Future state of the Antarctic Ice Sheet using CISM.** (a) Ice thickness change after a 1000-year continuation experiment initialized with present-day ocean thermal forcing. The original modeled GL resulting from the spin-up is shown in green, and the GL



**Deleted:**

**Deleted: 2**

**Formatted: Font: 9 pt**

**Formatted: Font: 9 pt**

**Formatted: Font: 9 pt**

**Deleted: mass change rates.**

**Formatted: Font: 9 pt**

855 position at  $t = 1000$  years is shown in black, only where it deviates from the spin-up GL. The thin grey lines show the modeled elevation  
 with an interval of 1000 m at  $t=1000$  years. (b) Ice mass above floatation for Thwaites Glacier (TG) and Pine Island Glacier (PIG) in blue,  
 relative to the initial state shown in Fig. 1, and the corresponding sea level **change** equivalent (calculated according to Eq 2 in Goelzer et al.  
 (2020) of TG, PIG (combined, crosses) and the AIS (stars) in red. Present-day observed mass loss is extrapolated in time and labeled as  
 860 extrapolated observations in black. (c) GL displacement over time, and the bedrock profile along cross section  $CD$ . The last ridge  
 before collapse is initiated,  $AB$ , is shown with a vertical black line. Once the GL passes this ridge, mass loss accelerates. A zoomed-in figure  
 including the 2D bedrock profile is shown in Extended Data Fig. S8.

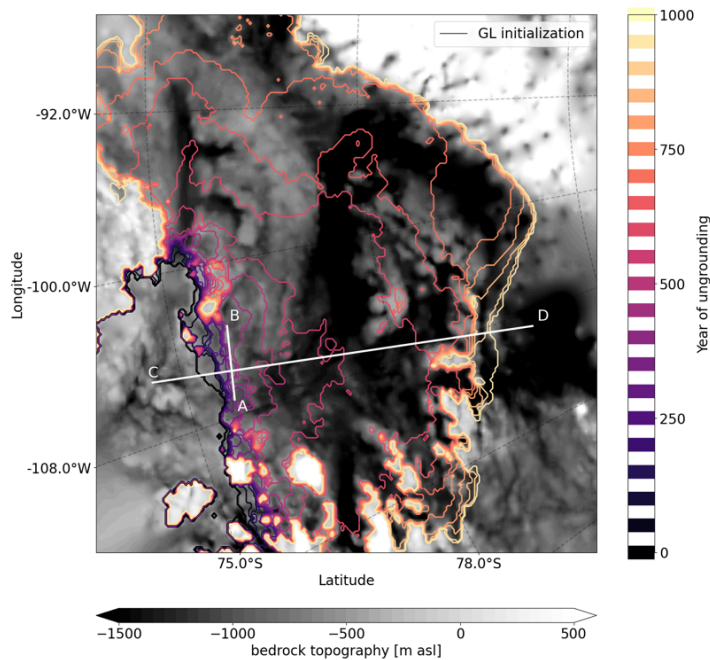


**Figure 4. ASE bedrock topography and grounding line migration of the future simulation.** The bedrock elevation (m) is shown with  
 865 grey shading. Magma contours show the grounding line position at different times during the default continuation experiment. Contour lines  
 clumped together highlight areas where the grounding line stabilizes for long periods. The short white line (AB) shows the last prominent  
 ridge before the accelerated collapse starts, and the long white semi-horizontal white line (CD) shows the location of the cross section plotted  
 in Fig. 2 in the main text.

Formatted: Font: 9 pt

Formatted: Font: 9 pt

Deleted: )

Formatted: Font: 9 pt

Deleted: S7

Formatted: Font: 9 pt

Formatted: Font: 9 pt

Deleted: After 400 years, the mass loss accelerates as both PIG and  
 TG collapse. The TG GL recedes faster than that of PIG (Fig. 2b).  
 After 500 years, when the collapse is under way



875 The TG GL recedes faster than that of PIG (Fig. 5b), in line with the mass loss above flotation (Fig 3b), where the TG mass loss acceleration precedes the PIG acceleration. In model year 500, ice velocities in the main channel of TG exceed 4000 m/yr, about twice the current modeled values (Fig. 5e). Thinning is greatest near the new GL, which is on a retrograde bed and therefore deeper than the current GL. Ocean thermal forcing in the ASE increases with depth, therefore newly ungrounded grid cells have a higher basal melt rate and thin rapidly. After 750 years, TG and PIG have collapsed, and the basins contain  
880 almost no grounded ice, except on a few small ridges with bedrock above sea level. A large, confined ice shelf has formed, with a thickness of several hundred meters near the GLs, decreasing to tens of meters near the (non-moving) calving front. At that time, the two basins have contributed about 1.2 meters to global mean sea level. Hence, the retreat of TG and PIG consists of two phases: a gradual decrease for the first few centuries, followed by an accelerated collapse, which continues until the basins are empty. PIG retreat is accelerated by the simultaneous collapse of TG. However, each glacier collapses on its own  
885 when the observed mass change rates are applied only to a single basins (not shown).

**Deleted:** 3e

**Deleted:** around

**Deleted:** Ocean thermal forcing in the ASE increases with depth since the melting point of ice decreases with increasing pressure (Jourdain et al., 2020); therefore newly ungrounded grid cells have a high basal melt rate and thin rapidly.

**Deleted:** instead.

**Deleted:** linear

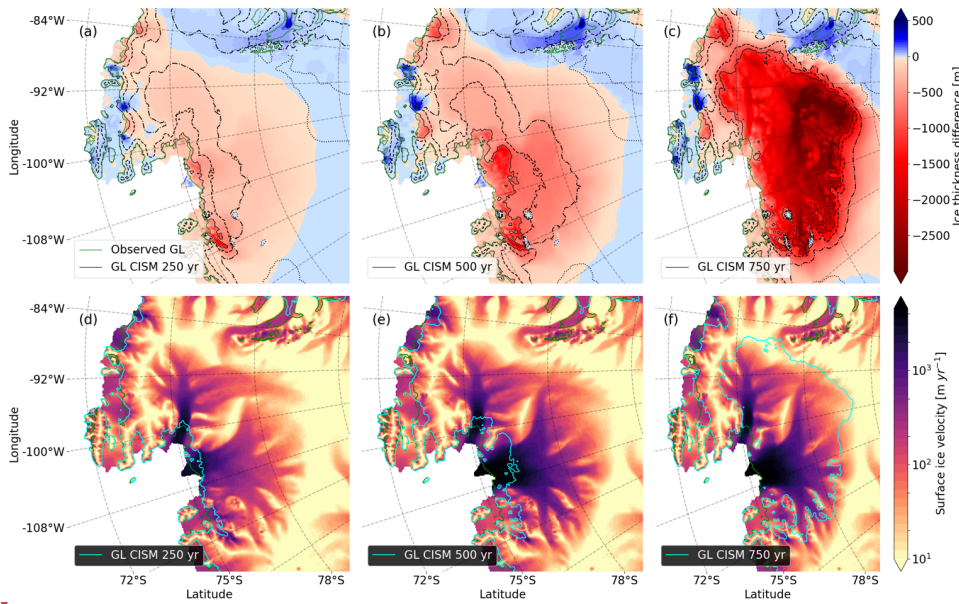
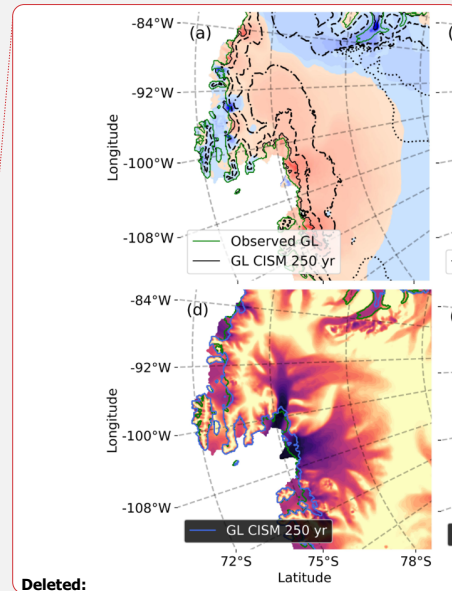


**Figure 5.** Development of the collapse at three times. (Top) Ice thickness difference with respect to the end of the initialization at  $t=250$  yr (a),  $t=500$  yr (b) and  $t=750$  yr (c) after the start of the default continuation experiment. The present-day GL from observations is shown in green, and the modeled GL is shown in black. The ice surface elevation lines are contours of 500 (dashed), 1000 (dash-dotted) and 2000 (dotted) meters. (Bottom) Ice surface velocities at  $t=250$  (d),  $t=500$  (e) and  $t=750$  (f) years, with the modeled GL shown in cyan, and the observed GL in green.

During the continuation experiment, the collapse can be halted by turning off basal melting completely (yellow lines in Fig. 6a). We observe two features in these zero basal melting experiments: the ice sheet re-advances more slowly than it collapsed, and the re-advance is slower when basal melt rates are switched off later during the simulation. Setting the basal melt rates to zero is equivalent to decreasing ocean temperatures up to 4 K near the GL and on average 2–3 K elsewhere. We also tested the effect of an instant cool-down of 1, 1.5 and 2 K at 250 years (brown lines) and 1.5, 2, 2.5 and 3K after 500 years (red lines) during the simulation. None of the cool-down experiments were enough to regrow the ice sheet to the initial condition on the same timescales as the retreat. Most of the experiments merely postpone the total collapse of the TG and PIG basins. Only a full basal melt stop will at any moment halt the collapse. We also tested a percentage decrease in basal melt rates at certain timesteps. Setting the basal melt rates to 75% and 50% of their present-day value (yellow and brown lines in Fig 6b) does not



Deleted:

Deleted: 3

Deleted: blue

Deleted: whole

Deleted: S8). This

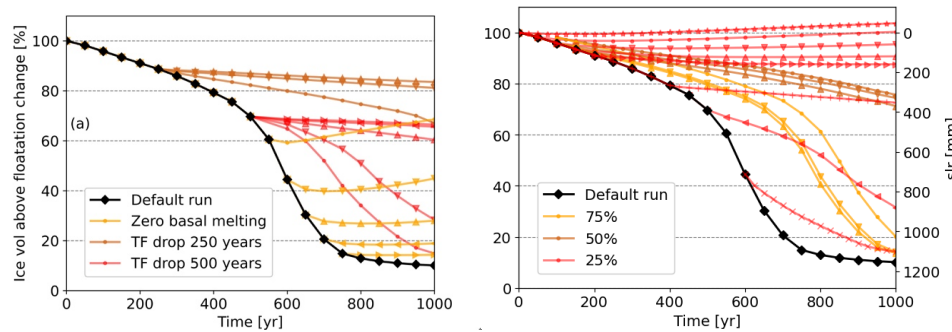
Deleted: To test whether the retreat is irreversible under realistic conditions, we ran experiments with ocean temperatures lowered at certain moments in the future. For example, the collapse can be stopped by cooling the ocean by 2 K relative to present-day values after ...

Deleted: . After

Deleted: ,

Deleted: can be stopped

stop the collapse, but only delays it. Setting melt rates of 25% (red lines) of their present-day value results in eventual regrowth, but only when applied in the first 200 years of the simulation (red lines in Fig 6b).



930 **Figure 6. The impact of decreasing basal melt rates on the ice retreat.** (Left) Evolution of ice volume (shown as a percentage relative to the initial volume (see Fig. 1) for PIG and TG combined and as sea-level equivalent on the right y-axis) over 1000 years in experiments with a sudden decrease in basal melt rates. Brown lines show where the thermal forcing (TF) is instantly decreased after 250 years by 1 K, 1.5 K and 2 K, and the red lines show simulations where the thermal forcing is decreased after 500 years by 1.5 K, 2 K, 2.5 K and 3 K. Yellow lines indicate runs where the basal melting is instantly switched off after 500, 600, 700 and 800 years. (Right) Percentage of the basal melt rates applied: 25% (red), 50% (brown) and 75% (yellow). The 50% and 75% basal melt rate experiments are started at 50, 100 and 150 years, and the 25% basal melt rate experiments are started at 0, 50, 100, 150, 200, 400, 500 and 600 years after the start of a transient continuation run.

940 The accelerated collapse resembles the MISI mechanism (Schoof, 2012, 2007). However, the analytical solution of Schoof (2012) and Schoof (2007) does not account for an initial buttressing shelf and is valid only when there is no change in buttressing. Recent studies have indicated that the current TG ice shelves provide little or no buttressing (Gudmundsson et al., 2023; Gudmundsson et al., 2019; Fürst et al., 2016). During and after the modeled collapse, a large buttressing ice shelf forms. This is at least partly because of our conservative stationary calving front, in reality the front might move inland from its present-day position. As a result, ongoing basal melting is needed to overcome the increased buttressing and sustain the retreat.

945 Removing the basal melt entirely would halt the collapse (see Fig. 6). This makes our retreat at least partly driven by forcing, and not strictly an unstable ice dynamical system, as would be the case in the theoretical non-buttressed MISI description.

It is still debated whether the presence of warm CDW, about 3–4 degrees K above the melting point (Jacobs et al., 2011b), under the PIG and TG shelves is a result of natural variability (Silvano et al., 2022) or forced by climate change (Holland et al., 2019). One model study (Holland et al., 2019) found that present-day WAIS basal melting is partly caused by internal

**Deleted:** by ocean cooling of more than 2.5

**Deleted:** .

**Formatted:** Font: 9 pt, English (UK)

**Formatted:** Font: 9 pt, English (UK)

**Formatted:** English (UK)

**Deleted:** Hence, the

**Deleted:** marine ice sheet instability (

**Deleted:** )

**Deleted:** (Schoof, 2012, Schoof and Hewitt, 2013).

**Deleted:** Schoof and Hewitt (2013)

**Deleted:** Recently, two studies indicated that the current TG ice shelves provide little to no buttressing (Gudmundsson et al., 2019, Gudmundsson et al., 2023). During and after the modeled collapse, however, a large ice shelf forms, providing significant buttressing.

**Deleted:** Stopping the basal melt would stop the collapse (see Fig. S8). Hence, we do not refer to the collapse as pure MISI following the analytical “Schoof” definition (Schoof, 2012), since the retreat would not proceed unabated if ocean thermal forcing were removed.

**Deleted:** (Jacobs et al., 2011)

**Deleted:** (Holland et al., 2019, Silvano et al., 2022) or forced by climate change.

970 variability and partly anthropogenically forced. In the case of natural variability, CDW might be (partly) absent in the future,  
lowering the melt rates. When we first run 50 years into the future with the default initialization and then instantly halve the  
975 melt rates, the collapse is delayed but not halted (Fig 6b).

### 5. Results: UFEMISM simulation

980 The default experiment shown in Fig. 3 is repeated with the ice sheet model UFEMISM. The initialized state of the UFEMISM  
simulation is shown in Figure S4, in terms of ice thickness and ice surface velocity differences with present-day observations.  
985 The inverted quantities are shown in Figure S5. Figure 7 shows the result of an unforced continuation simulation with  
UFEMISM, initialized with the present-day mass loss rates and using PMP at the grounding line. The run setup is very similar  
to the default experiment using CISM but differs, as mentioned in Sect. 2.4, in the stress balance, discretization, sliding law,  
and grounding line parameterizations.

990 The ice thickness change shown in Figure 7 is again dominated by the collapse of Thwaites and Pine Island Glacier, just as in  
the default CISM simulation shown in Figure 3. The same floating corridor has formed at the Rutford ice stream, connecting  
the Amundsen Sea and the Filchner-Ronne ice shelf. The Antarctic Peninsula is still connected to the Bellingshausen sector  
via grounded ice, a feature that is absent in the CISM simulation shown in Figure 2. The UFEMISM simulation predicts slightly  
less grounding line retreat. On the remaining AIS, the ice thickness change is largely negative and close to zero (on the order  
of 1–5 meters of total ice thickness change over 1000 years), with the exception of some small outlet glaciers in Dronning  
Maud land. The mass change patterns on the Ross and Filchner–Ronne ice shelves match the patterns shown in Figure 3. We  
therefore conclude that the ASE collapse is likely not restricted to CISM, but rather the result of initializing an ice sheet model  
with the present-day mass change rates.

**Deleted:** former

**Deleted:** We therefore tested a range of values of ocean forcing and melt rates.

**Deleted:** halved

**Deleted:** This suggests that if as much as half of the current basal melting is anthropogenically forced (e.g., from increased greenhouse gases and/or reduced stratospheric ozone), TG and PIG are still vulnerable to collapse.

**Deleted:** 5

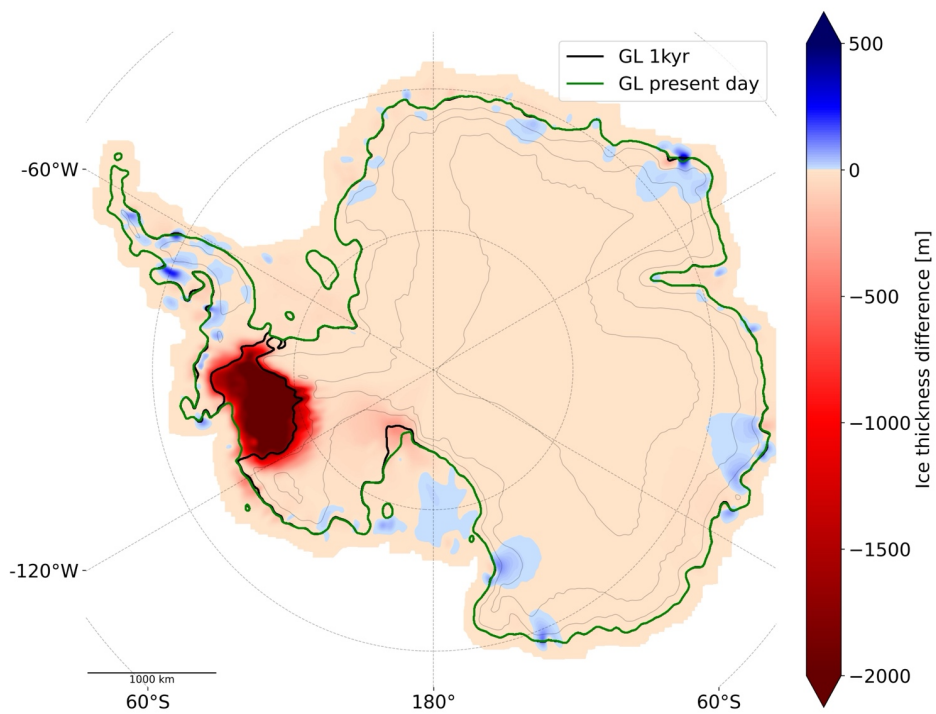


**Figure 7. Future state of the Antarctic Ice Sheet using UFEMISM.** Ice thickness change after a 1000-year continuation experiment initialized with present-day mass change rates. The original modeled GL resulting from the spin-up is shown in green, and the GL position at  $t = 1000$  years is shown in black, only where it deviates from the spin-up GL. For this figure, the UFEMISM data on an irregular triangular

005 grid were interpolated to the same regular rectangular grid as is used in the CISM simulations, and smoothed with a Gaussian kernel for visibility.

## 6. Model choices and parameter value exploration

010 The results presented in Section 4 are based on the best estimate of the current system state, and a single set of preferred model physics choices and parameter values. To assess the sensitivity of the model, we varied many of these choices within the range we viewed as physically realistic. The aim of these experiments is to determine which processes and parameter choices can either accelerate or slow (and perhaps prevent) the projected collapse. Where appropriate, we redid the transient initialization with the new choices (runs with an "\*" in Table 3). In other cases, we recomputed free parameters to start from the same  
015 initialized state (same ice thickness and velocities, and initial dh/dt) as our default experiment, to minimize the effect of a slightly different initialized state. We verified for the simulations starting with a new initialization that there is little model drift, and that PIG and TG would not collapse without applying the mass change rates.

Figure 8 and Table 3 show the relative mass loss and resulting GMSL rise relative to the initial state for this set of model choices and parameter values. Notably, the continuation of present-day climate forcing leads to TG and PIG collapse in all experiments, except the default simulation without applying the present-day mass change rates (the model drift experiment, dashed line in Figure 8). In this experiment, PIG starts to readvance to a downstream seabed ridge, creating some positive model drift.

025 Once a collapse is initiated (i.e., when the mass loss accelerates), mass loss rates are similar, and all experiments show a similar collapse duration (150–250 years, see Table 3). During the fast phase, the mass loss rate is about 3 mm GMSL/yr for almost every experiment. This is irrespective of the parameter setting, suggesting that the collapse rate during the fast phase is controlled by the bed topography and/or internal system dynamics rather than detailed physics or parameter choices.

030 The collapse timing is insensitive to the basal friction law (in line with Barnes and Gudmundsson (2022), model resolution (8 km or 4 km), and a 20% increase in the integrated SMB. Also, glacial isostatic adjustment (GIA), estimated using an Elastic Lithosphere Relaxing Asthenosphere (ELRA) model (Lambeck and Nakiboglu, 1980) with a relaxation time of 3000 yr, has little impact on glacier stability. GIA with a very short relaxation time of 100 yr delays the collapse by several centuries but does not prevent it. These findings are similar to those of Berdahl et al. (2023).

The collapse timing is sensitive to model choices related to basal melting. A weaker/stronger dependence of the basal melt on the thermal forcing at the ice draft depth (Jourdain et al., 2020), i.e. a higher/lower value for  $\gamma_0$  in Eq (1.5), delays/advances the start of the collapse (as in Berdahl et al. 2023). Allowing no melt in a grid cell containing the GL (NMP) instead of partial melt (PMP) delays the collapse for several centuries, but does not prevent a collapse.

Deleted: , the

Deleted: parameterizations and their optimal

Deleted: setting

Deleted: if

Deleted: results are robust

Deleted: observational and model uncertainties, we picked of each source of uncertainty, values that are on the edge of being

Deleted: find

Deleted: process

Deleted: , hence might indicate that the default evolution of collapse is incorrect.

Deleted: 4

Deleted: .

Deleted: the same

Deleted: –

Deleted: reaches

Deleted: (Barnes and Gudmundsson, 2022), model resolution (8 km or 4 km), and a 20% increase in the integrated SMB.

Deleted: These findings are similar to the ones in Berdahl et al. (2023). ...

Deleted: Taking a conservative approach by assuming

The UFEMISM simulations show a similar pattern of mass loss as the CISM simulations. Again, there is a gradual linear phase of ice mass loss. When approximately 30% of the original ice mass above floatation in the ASE has disappeared, the accelerated collapse begins; this phase lasts approximately 200 years with FCMP and 250 years with NMP. The similar behavior of the UFEMISM simulations suggests it is unlikely that the WAIS collapse modelled in CISM is a model artifact. The timing on the start of the collapse differs in our sensitivity experiment with about 1200 years. The large difference in collapse timing highlights that the choice of ice sheet model is a major source of uncertainty.

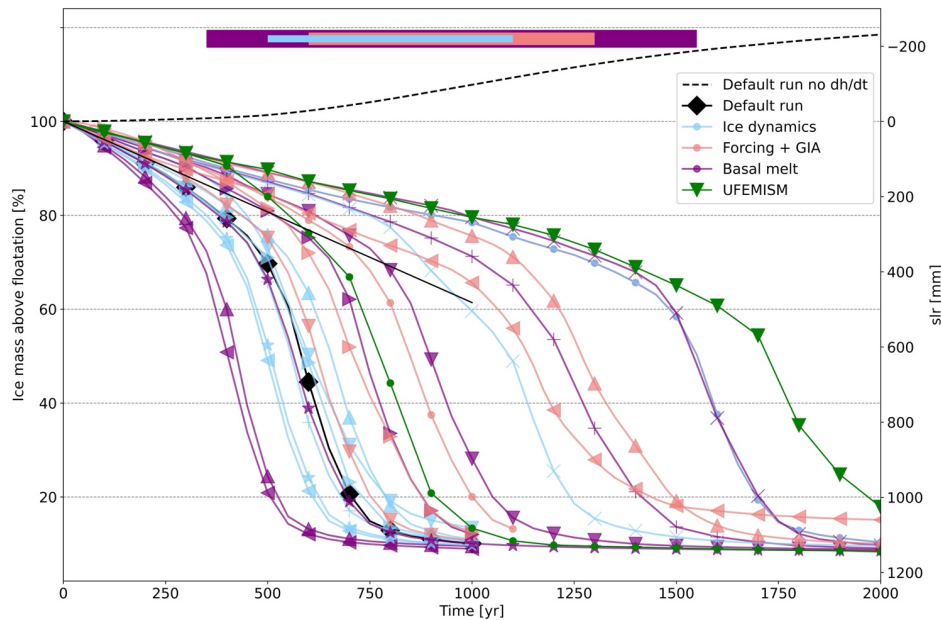


**Figure 8. Sensitivity analysis.** Ice mass above floatation (left y-axis) and resulting sea level rise (right axis) in the combined Thwaites and Pine Island Glacier basins for different experiments (22 in total). The mass change is calculated as the percentage difference relative to the initial value in the TG and PIG basins. The default run shown in Fig. 3 is plotted with black diamonds. The same run without applying the present-day mass change rates, i.e. the model drift experiment, is shown as a dashed line. The UFEMISM runs are shown in green, and the extrapolated observations as in Fig. 2b are shown in marker-free black. Most runs start with the observed mass change rates but deviate early in the run due to dynamic feedbacks. Some runs, e.g. “SMB increases by 20% instantly” start with different mass change rates. This explains the spreading trajectories in the first 100 years. The colored bars at the top indicate the range of times that the simulations reach 50% of their present-day ice volume, to highlight the uncertainty related to different categories. See Table 3 for a description of each run.

Deleted: conducted using CISM.

Deleted: a

Deleted: is modeled, and when

Deleted: is initiated which

Deleted: when employing

Deleted: when employing

Deleted: -dependent feature, but

Deleted: timing of the

Deleted: the largest

Deleted: in this study with respect to the timing of the collapse

Moved down [9]: It would be interesting to study simultaneous changes in multiple parameters and physical choices. However, when combining two conservative model choices, e.g.

Moved down [10]: To generate a single conservative end-member, we combined the two most conservative runs (“No-melt parameterization at the GL” and “ELRA isostasy, relaxation time = 100 years” in Table 1) into a “most conservative estimate.” In this simulation, TG and PIG collapse after 2500 years (not shown in Fig.

Deleted: ¶

In all simulations, there is first a nearly linear grounding line retreat with WAIS mass loss similar to the present day. This slow retreat phase is followed by accelerated retreat leading to Pine Island and Thwaites collapse. This behavior is in line with several earlier papers that did not include present-day mass change rates and therefore had to rely, for example, on ocean temperature (basal melt rate) perturbations (Joughin et al., 2014, Arthern and Williams, 2017, Golledge et al., 2021, Coulon et al., 2023). The ice loss rate ¶ [14]

Deleted: NMP and low melt sensitivity to thermal forcing. (... [15]

Deleted: 4). ¶ (... [16]

Deleted: 4

Formatted: Font: 9 pt

Formatted: Font: 9 pt

Deleted: for

Deleted: areas highlighted in Fig. 1a by orange polygons.

Deleted: 2

Formatted: Font: 9 pt

Formatted: Font: 9 pt

Formatted: Font: 9 pt

Formatted: Font: 9 pt

Formatted: Font: 8 pt

Formatted: Font: 9 pt

Deleted: 1

Formatted: Font: 9 pt

Deleted: ¶ (... [17]

140 **Table 3. Summary of the sensitivity experiments.** Descriptions of the runs shown in Fig. 4. Except as noted otherwise, all settings and  
resolutions are the same as for the default initialization and continuation run. For some runs, denoted by an <sup>“\*”</sup>, a new initialized state was  
needed. This new initial state is tested on model drift, and verified that a PIG and TG collapse was not found when not applying the present-  
145 day mass change rates. An extended description of each run can be found in Extended Data Table S1. The year of collapse initiation is  
defined as the year when the rate of basin-wide mass loss exceeds a 10% change in initial mass per 75 years (0.13%/year), which is equivalent  
to 1.72 mm GMSL/yr. The end of the collapse is defined as the first time the mass loss drops below this threshold again.

Formatted: Font: 9 pt

Deleted: asterisk\*,

Formatted: Font: 9 pt

Formatted: Font: 9 pt
























Formatted: Font: 9 pt

Deleted:

Formatted: Font: 9 pt

Formatted: Font: 9 pt, Not Bold



<u>Run description (full description in Extended Data Table 1)</u>	<u>collapse initiated [yr]</u> <u>(avg SLR rate [mm/yr])</u>	<u>collapse completed [yr]</u> <u>(max SLR rate [mm/yr])</u>	<u>Marker</u>
<u>8km grid, partial melt parameterization (Leguy et al., 2021) *</u>	<u>300 (3.45)</u>	<u>500 (4.41)</u>	
<u>Highest basal melt versus depth sensitivity from Jourdain et al. (2020)</u>	<u>300 (3.06)</u>	<u>550 (5.32)</u>	
<u>Larger flow factor (softer ice) *</u>	<u>400 (3.22)</u>	<u>600 (4.24)</u>	
<u>No ocean connection (p=0, Eq. 1.3) (Leguy et al., 2021)</u>	<u>400 (2.74)</u>	<u>650 (4.24)</u>	
<u>With Schoof basal sliding parameterization, based on (Asay-Davis et al., 2016)</u>	<u>450 (2.66)</u>	<u>650 (4.33)</u>	
<u>Thermal forcing capped at the maximum found at the GL</u>	<u>500 (2.69)</u>	<u>700 (3.9)</u>	
<u>Default continuation experiment</u>	<u>500 (2.95)</u>	<u>700 (4.15)</u>	
<u>ELRA isostasy, relaxation time = 3000 years</u>	<u>500 (2.26)</u>	<u>700 (3.28)</u>	
<u>With a Weertman power-law basal sliding parameterization</u>	<u>450 (2.51)</u>	<u>700 (3.01)</u>	
<u>SMB increases by 20% instantly</u>	<u>500 (2.72)</u>	<u>750 (3.95)</u>	
<u>Smaller flow factor (stiffer ice) *</u>	<u>550 (2.54)</u>	<u>800 (3.82)</u>	
<u>Mass change rates applied only on ice shelves*</u>	<u>600 (2.16)</u>	<u>900 (3.18)</u>	
<u>8-km grid, flotation-condition melt parameterization (Leguy et al., 2021)*</u>	<u>650 (2.5)</u>	<u>900 (4.07)</u>	
<u>Decrease basal melt rates after 50 years by 25%</u>	<u>700 (2.39)</u>	<u>950 (3.15)</u>	
<u>UFEMISM, partial melt parameterization*</u>	<u>700 (2.02)</u>	<u>900 (3.06)</u>	
<u>Flotation condition melt parameterization (Leguy et al., 2021)*</u>	<u>800 (2.36)</u>	<u>1050 (3.12)</u>	
<u>ELRA isostasy, relaxation time = 100 years</u>	<u>1100 (2.72)</u>	<u>1200 (2.2)</u>	
<u>Full ocean connection (p=1, Eq. 1.3) (Leguy et al., 2021)</u>	<u>1100 (1.82)</u>	<u>1250 (2.85)</u>	
<u>Lowest basal melt versus thermal forcing sensitivity from ref. (Jourdain et al., 2020)</u>	<u>1200 (2.72)</u>	<u>1400 (3.48)</u>	
<u>Decrease basal melt rates after 50 years by 50%</u>	<u>1200 (2.09)</u>	<u>1350 (2.59)</u>	
<u>No-melt parameterization at the GL (Leguy et al., 2021) *</u>	<u>1500 (2.31)</u>	<u>1700 (3.29)</u>	
<u>8-km grid, no-melt parameterization (Leguy et al., 2021) *</u>	<u>1500 (2.15)</u>	<u>1700 (2.95)</u>	
<u>UFEMISM, flotation-condition melt parameterization *</u>	<u>1600 (1.94)</u>	<u>1850 (2.50)</u>	

## 7. Discussion

155 We have developed a modified ice sheet initialization method and applied it in Antarctic Ice Sheet simulations using two models, CISM and UFEMISM. This method enables an ice sheet model to be spun up to a state consistent with the observed ice sheet geometry, while also matching the observed mass change rates. Previous initialization methods were unable to capture the observed mass change rates; this was a shortcoming compared to data assimilation initialization methods.

160 In model simulations spanning a wide range of physics and parameter choices, Thwaites Glacier and Pine Island Glacier collapse on a timescale of several centuries without additional climate forcing beyond the ocean forcing required to match present-day melt rates. In other words, the present ocean-driven mass imbalance is a precursor for large-scale deglaciation of the WAIS. A period of gradual retreat over several centuries is followed by a phase of rapid collapse over about two centuries, with GMSL rising by about 3 mm yr<sup>-1</sup> during the collapse phase. This behavior, including the collapse rate, is consistent with several previous studies (Joughin et al. (2014); Golleddge et al. (2021); Coulon et al. (2024); Feldmann and Levermann (2015)).  
165 The timing of collapse initiation differs widely across our experiments, as well as in previous studies, and remains a source of large uncertainty (Fig 8).

170 Each sensitivity experiment (Table 3) varies a single parameter or physics choice relative to the default experiment. It would be interesting to study simultaneous changes in multiple parameters and physical choices. However, when combining two conservative model choices, e.g. NMP and low melt sensitivity to thermal forcing, the inversion procedure often fails to reproduce the observed GL location, suggesting that the combination is unrealistic. For this reason, and because most combinations require a separate, computationally expensive initialization, we did not consider these combined effects. To generate a single conservative end-member, we combined the two most conservative runs (“No-melt parameterization at the GL” and “ELRA isostasy, relaxation time = 100 years” in Table 1) into a “most conservative estimate.” In this simulation, TG and PIG collapse after 2500 years (not shown in Fig. 8). Applying no melt in a cell containing the grounding line is conservative, since the transition between grounded and floating ice occurs over an extended grounding zone possibly influenced by tides (Graham et al., 2022).

180 We note three missing processes that could affect the ice evolution. First, the mass change rates on grounded ice are controlled by parameters in the basal sliding law, which are not necessarily constant over time. After the initialization phase,  $C_c$  is kept constant during forward runs, not accounting for future evolution of the ice–bed interface, such as increased basal meltwater that could enhance sliding (Kazmierczak et al., 2024). In addition, possible feedbacks between the ice flow and the bed (e.g. Rémy and Legresy (2004); Van Der Wel et al. (2013)) are only partly represented by the basal friction law and the calculation of the effective pressure on bedrock below sea level, representing the hydrological connection to the ocean.

185 Second, as ice shelves melt and retreat, they add freshwater to the ocean, but the current model setup ignores the potential feedback of the additional fresh water on ocean temperature or salinity. There are several ways for the freshwater flux from a

Moved (insertion) [9]

Moved (insertion) [10]

Moved (insertion) [6]

Moved (insertion) [7]

190 collapsing WAIS to influence the ocean properties of the Amundsen Sea and the Southern Ocean. For example, increased freshwater can cool the Southern Ocean sea surface (Bintanja et al., 2015) and reduce Antarctic Bottom Water formation (Williams et al., 2016). Alternatively, the freshwater input can stratify the ocean just beyond the shelves, thus trapping heat in the subsurface ocean and ultimately increasing heat transport into cavities, resulting in higher basal melt rates (Flexas et al., 2022). It has also been suggested that interactions between freshwater flux and sea ice formation and the presence of warm, dense water in large AIS cavities can stabilize and stratify the ocean flow in cavities, preventing further warm water from flowing into the cavity (Hellmer, 2004). Hence, the exact effect of a large freshwater pulse into the ocean surrounding the AIS remains unknown based on model studies (Swart et al. (2023)). Since we use a standalone-ice sheet model in this study, and no consensus has been reached on the effect of the freshwater flux, we did not parameterize this effect. In future studies, freshwater feedbacks could be added by coupling the ice sheet model to a cavity-resolving ocean model.

200 Third, bedrock uplifting could slow down glacier retreat in MISI-prone areas (Book et al., 2022; Kachuck et al., 2020; Van Calcar et al., 2023). In our default experiment, we do not simulate bedrock height changes. We perform sensitivity tests with CISM's ELRA model of glacial isostasy in Section 6. However, these experiments assume, perhaps unrealistically, that the bedrock is in equilibrium at the start of the forward simulation.

Moved (insertion) [8]

Deleted: 6. Conclusions and outlook\*

## 7. Conclusions and outlook

We have developed a method to incorporate present-day mass change rates in an Antarctic Ice Sheet model initialization using a spin-up. Given these observed rates, we show that for a wide range of model choices, Thwaites Glacier and Pine Island Glacier will ultimately collapse, likely within 1000 years. These results are consistent with several previous studies but carried out with an improved initialization scheme, a much wider range of model configurations, and without additional climate forcing. The timing of collapse onset is highly dependent on model details and varies in our study from 300 to 2500 years. The length of the fast collapse phase (about 200 years) and the maximum mass loss during the collapse (~ 3 mm SLE yr<sup>-1</sup>), are consistent across experiments. These experiments suggest that eventual collapse is inevitable for the current climate and can probably be averted only by a large decrease in sub-shelf ocean temperatures. The collapse will likely begin sooner if Amundsen sub-shelf cavities were to warm further in the next few decades, as projected by a recent ocean modelling study (Naughten et al., 2023).

The present-day observed imbalance in the ASE is likely caused by the presence of warm ocean conditions, and the current ice sheet geometry is reacting to higher basal melt rates and the loss of buttressing. While some of the warming may be the result of natural variability, it is plausible that the cavities warmed during the past century when a different geometry was present. In that case, GCMs and high-resolution regional models could be used to simulate the coupled ice–ocean–atmosphere processes that might have triggered the recent warming. These models could also explore whether future anthropogenic action could cool these cavities enough to prevent collapse. Replication of our experiments with other ice sheet models could show that the collapse of Thwaites and Pine Island Glaciers is indeed unavoidable without a considerable reduction of basal melt. Alternatively, other models produce states for which the current mass loss ceases, and TG and PIG do not collapse.

### Code availability

CISM is an open-source code developed on the Earth System Community Model Portal (EPSCOMB) Git repository available at <https://github.com/ESCOMP/CISM>. The specific version used to run these experiments is tagged under [https://github.com/ESCOMP/CISM/releases/tag/dhdt\\_version](https://github.com/ESCOMP/CISM/releases/tag/dhdt_version).

### Data availability

The input dataset, the default initialization and the output of all experiments shown in Table 3 can be found at Zenodo <https://zenodo.org/records/13897556>, DOI: 10.5281/zenodo.13897556

Deleted: new

Deleted: AIS

Deleted: (conservative)

Deleted: These results are consistent with several previous studies (e.g., (Favier et al., 2014, Joughin et al., 2014),

Deleted: sensitive to

Deleted: potential natural variability

Deleted: ocean temperatures, but the

Deleted: ,

Deleted: , is not. This

Deleted: is irreversible

Deleted: Since

Deleted: subsequently

Deleted: in ASE cavities do not seem to

Deleted: able to coexist with the present-day geometry in steady state...

Deleted: likely

Deleted: confirm our results and perhaps better constrain the timing of the collapse. We hypothesize that other models, like CISM and UFEMISM, will simulate collapse of TG and PIG on timescales of several centuries if the ocean forcing is sufficient to reproduce present-day thinning rates.

Deleted: ¶

¶ Data and code

Deleted: Datasets used as input or calibration: bedrock profile and ice thickness from Morlighem et al. (2020), ice surface velocities from Rignot et al. (2019), ocean temperatures from Jourdain et al. (2020), surface mass balance from Van Wessem et al. (2018), geothermal heat flux from Martos et al. (2017), and mass changes rates from Smith et al. (2020) . ¶ The Community Ice Sheet Model 2.1.1 (CISM) and the Utrecht Finite Volume Ice-Sheet model UFEMISM v1.0 are both freely available on GitHub. ...

### Author contributions

1280 Tvda designed and executed the main experiments and the sensitivity analysis. WHL and GRL developed CISM and helped  
configure the model for the experiments. CJB and JAB performed the UFEMISM experiments and processed the data for the  
sensitivity analysis. RSWvdW and WJvdB provided guidance and feedback. Tvda prepared the manuscript, with contributions  
from all authors.

1285 Tvda received funding from the NPP programme of the NWO. WHL and GRL were supported by the NSF National Center  
for Atmospheric Research, which is a major facility sponsored by the National Science Foundation (NSF) under Cooperative  
Agreement no. 1852977. Computing and data storage resources for CISM simulations, including the Cheyenne supercomputer  
(<https://doi.org/10.5065/D6RX99HX>), were provided by the Computational and Information Systems Laboratory (CISL) at  
NSF NCAR. GRL received additional support from NSF grant no. 2045075. CJB was supported by PROTECT. This project  
has received funding from the European Union's Horizon 2020 research and innovation program under grant agreement no.  
1290 869304. JB received funding from NWO grant 515.

The authors declare no competing interests.

### References

- 295 Adusumilli, S., Fricker, [H. A.](#), Medley, [B.](#), Padman, [L.](#), and Siegfried, [M. R.](#): Interannual variations in meltwater input to the  
Southern Ocean from Antarctic ice shelves, *Nature geoscience*, **13**, 616-620, [2020](#).
- Amaral, T., Bartholomäus, [T. C.](#), and Enderlin, [E. M.](#): Evaluation of iceberg calving models against observations from  
Greenland outlet glaciers, *Journal of Geophysical Research: Earth Surface*, **125**, e2019JF005444, [2020](#).
- Arthern, R. J. and Williams, [C. R.](#): The sensitivity of West Antarctica to the submarine melting feedback, *Geophysical  
Research Letters*, **44**, 2352-2359, [2017](#).
- 300 [Arthern, R. J.](#), [Hindmarsh, R. C.](#), and [Williams, C. R.](#): Flow speed within the Antarctic ice sheet and its controls inferred from  
satellite observations, *Journal of Geophysical Research: Earth Surface*, **120**, 1171-1188, [2015](#).
- Asay-Davis, X. S., Cornford, [S. L.](#), Durand, [G.](#), Galton-Fenzi, [B. K.](#), Gladstone, [R. M.](#), Gudmundsson, [G. H.](#), Hattermann, [T.](#),  
Holland, [D. M.](#), Holland, [D.](#), and Holland, [P. R.](#): Experimental design for three interrelated marine ice sheet and ocean model  
intercomparison projects: MISMIP v. 3 (MISMIP+), ISOMIP v. 2 (ISOMIP+) and MISOMIP v. 1 (MISOMIP1), *Geoscientific  
Model Development*, **9**, 2471-2497, [2016](#).
- 305 Aschwanden, A., [Aðalgeirsdóttir, G.](#), and [Khroulev, C.](#): Hindcasting to measure ice sheet model sensitivity to initial states,  
*The Cryosphere*, **7**, 1083-1093, [2013](#).
- [Aschwanden, A.](#), [Bartholomäus, T. C.](#), [Brinkerhoff, D. J.](#), and [Truffer, M.](#): Brief communication: A roadmap towards credible  
projections of ice sheet contribution to sea level, *The Cryosphere*, **15**, 5705-5715, [2021](#).

Formatted: Font: Bold

Deleted: H. A. ...ricker, B.... A., Medley, L....., Padman, L., and  
M. R. ...iegfried (2020). "... M. R.: Interannual variations in  
meltwater input to the Southern Ocean from Antarctic ice sh... [18]

Deleted: (9):

Formatted ... [19]

Deleted: T. C. ...artholomäus, T. C., and E. M. ...nderlin (2020).  
"... E. M.: Evaluation of iceberg calving models against observations  
from Greenland outlet glaciers." ... [20]

Deleted: (6):

Formatted ... [21]

Deleted: C. R. ...illiams (2017). "... C. R.: The sensitivity of West  
Antarctica to the submarine melting feedback." ... [22]

Formatted ... [23]

Deleted: (5):

Deleted: S. L. ...ornford, G..... L., Durand, B. K....., Galton-Fenzi,  
R. M..... K., Gladstone, G. H..... M., Gudmundsson, T..... H.,  
Hattermann, D. M....., Holland, D. M., Holland, D., and P. R.  
Holland (2016). "... P. R.: Experimental design for three interrelated  
marine ice sheet and ocean model intercomparison projects: MISMIP  
v. 3 (MISMIP+), ISOMIP v. 2 (ISOMIP+) and MISOMIP v. 1  
(MISOMIP1)..." ... [24]

Formatted ... [25]

Deleted: (7):

Deleted: T. ...ðalgeirsdóttir, G., and Khroulev, C. ... [26]

Deleted: D. J..... C., Brinkerhoff, D. J., and M. ...ruffer (2021).  
"... M.: Brief communication: A roadmap towards credible  
projections of ice sheet contribution to sea level." ... [27]

Deleted: (12):

Formatted ... [28]

Barnes, J. M. and Gudmundsson, G. H.: The predictive power of ice sheet models and the regional sensitivity of ice loss to basal sliding parameterisations: a case study of Pine Island and Thwaites glaciers, West Antarctica, *The Cryosphere*, **16**, 4291-4304, 2022.

Benn, D. I., Cowton, T., Todd, J., and Luckman, A.: Glacier calving in Greenland, *Current Climate Change Reports*, **3**, 282-290, 2017.

Berdahl, M., Leguy, G., Lipscomb, W. H., Urban, N. M., and Hoffman, M. J.: Exploring ice sheet model sensitivity to ocean thermal forcing and basal sliding using the Community Ice Sheet Model (CISM), *The Cryosphere*, **17**, 1513-1543, 2023.

Berends, C. J., Goelzer, H., and Van De Wal, R. S.: The Utrecht finite volume ice-sheet model: UFEMISM (version 1.0), *Geoscientific Model Development*, **14**, 2443-2470, 2021.

Berends, C. J., Goelzer, H., Reerink, T. J., Stap, L. B., and Van De Wal, R. S.: Benchmarking the vertically integrated ice-sheet model IMAU-ICE (version 2.0), *Geoscientific Model Development*, **15**, 5667-5688, 2022.

Bernales, J., Rogozhina, I., and Thomas, M.: Melting and freezing under Antarctic ice shelves from a combination of ice-sheet modelling and observations, *Journal of Glaciology*, **63**, 731-744, 2017a.

Bernales, J., Rogozhina, I., Greve, R., and Thomas, M.: Comparison of hybrid schemes for the combination of shallow approximations in numerical simulations of the Antarctic Ice Sheet, *The Cryosphere*, **11**, 247-265, 2017b.

Bett, D. T., Bradley, A. T., Williams, C. R., Holland, P. R., Arthern, R. J., and Goldberg, D. N.: Coupled ice/ocean interactions during the future retreat of West Antarctic ice streams, *The Cryosphere Discussions*, 2023, 1-28, 2023.

Bintanja, R., Van Oldenborgh, G., and Katsman, C.: The effect of increased fresh water from Antarctic ice shelves on future trends in Antarctic sea ice, *Annals of Glaciology*, **56**, 120-126, 2015.

Book, C., Hoffman, M. J., Kachuck, S. B., Hillebrand, T. R., Price, S. F., Perego, M., and Bassis, J. N.: Stabilizing effect of bedrock uplift on retreat of Thwaites Glacier, Antarctica, at centennial timescales, *Earth and Planetary Science Letters*, **597**, 117798, 2022.

Bradley, A. and Arthern, R.: WAVI: A Fast, Flexible, and Friendly Modular Ice Sheet Model. Written in Julia, AGU Fall Meeting Abstracts, C11A-03.

Bueler, E. and Brown, J.: Shallow shelf approximation as a "sliding law" in a thermomechanically coupled ice sheet model, *Journal of Geophysical Research: Earth Surface*, **114**, 2009.

Cornford, S. L., Martin, D., Payne, A., Ng, E., Le Brocq, A., Gladstone, R. M., Edwards, T. L., Shannon, S. R., Agosta, C., and van den Broeke, M. R.: Century-scale simulations of the response of the West Antarctic Ice Sheet to a warming climate, *The Cryosphere*, **9**, 1579-1600, 2015.

Coulon, V., Klöse, A. K., Kittel, C., Edwards, T., Turner, F., Winkelmann, R., and Pattyn, F.: Disentangling the drivers of future Antarctic ice loss with a historically calibrated ice-sheet model, *The Cryosphere*, **18**, 653-681, 2024.

Danabasoglu, G., Lamarque, J. F., Bacmeister, J., Bailey, D., DuVivier, A., Edwards, J., Emmons, J., Fasullo, J., Garcia, R., and Gettelman, A.: The community earth system model version 2 (CESM2), *Journal of Advances in Modeling Earth Systems*, **12**, e2019MS001916, 2020.

Durand, G., Gagliardini, O., De Fleurian, B., Zwinger, T., and Le Meur, E.: Marine ice sheet dynamics: Hysteresis and neutral equilibrium, *Journal of Geophysical Research: Earth Surface*, **114**, 2009.

Favier, L., Durand, G., Cornford, S. L., Gudmundsson, G. H., Gagliardini, O., Gillet-Chaulet, F., Zwinger, T., Payne, A., and Le Brocq, A. M.: Retreat of Pine Island Glacier controlled by marine ice-sheet instability, *Nature Climate Change*, **4**, 117-121, 2014.

Feldmann, J. and Levermann, A.: Collapse of the West Antarctic Ice Sheet after local destabilization of the Amundsen Basin, *Proceedings of the national academy of sciences*, **112**, 14191-14196, 2015.

Flexas, M. M., Thompson, A. F., Schodlok, M. P., Zhang, H., and Speer, K.: Antarctic Peninsula warming triggers enhanced basal melt rates throughout West Antarctica, *Science advances*, **8**, eabj9134, 2022.

Fox-Kemper, B., H. T. Hewitt, C. X., Aðalgeirsdóttir, G., Drijfhout, S. S., Edwards, T. L., Gollidge, N. R., Hemer, M., Kopp, R. E., Krinner, G., Mix, A., Notz, D., Nowicki, S., Nurhati, I. S., Ruiz, J., Sallée, J.-B., Slangen, A. B. A., and Yu, Y.: Ocean, Cryosphere and Sea Level Change. In *Climate Change 2021: The Physical Science Basis. Contribution of Working Group I to the Sixth Assessment Report of the Intergovernmental Panel on Climate Change* Cambridge University Press, Cambridge, United Kingdom and New York, NY, USA, 1211-1362, 2021.

Fürst, J. J., Durand, G., Gillet-Chaulet, F., Tavaré, L., Rankl, M., Braun, M., and Gagliardini, O.: The safety band of Antarctic ice shelves, *Nature Climate Change*, **6**, 479-482, 2016.

- Deleted: G. H....Gudmundsson (2022), "... G. H.: The pr... [29]
- Deleted: (10):
- Formatted [30]
- Deleted: G. ...eguy, W. H...., Lipscomb, N. M.... H., Ur... [31]
- Deleted: (4):
- Formatted [32]
- Deleted: H. ...oelzer, T. J. Reerink, L. B. Stap...., and R. ... [33]
- Deleted: )" *Geoscientific Model Development* **15**(14): 56... [34]
- Deleted: **14**(5): 2443-2470
- Formatted [35]
- Deleted: I. ...ogozhina, R. Greve...., and M. ...omas (20... [36]
- Deleted: "
- Deleted: (1):
- Formatted [37]
- Deleted: Bernales, ...ett, D. T., Bradley, A. T., Williams, ... [38]
- Deleted: freezing under ...atsman, C.: The effect of increa... [39]
- Deleted: **63**(240): 731-744
- Formatted [40]
- Deleted: Bradley, A. ...ook, C., Hoffman, M. J., Kachuck... [41]
- Deleted: (2021).
- Deleted: ... AGU Fall Meeting Abstracts. [43]
- Formatted [42]
- Deleted: J. ...rown (2009), "... J.: Shallow shelf approxim... [44]
- Deleted: (F3)
- Formatted [45]
- Deleted: D. ...artin, A...., Payne, E...., Ng, A...., Le Br... [46]
- Deleted: (4):
- Formatted [47]
- Deleted: A. K. ...lose, C.... K., Kittel, R...., Edwards, T... [48]
- Deleted: J. F. ...amarque, J. F., Bacmeister, D...., Bailey... [49]
- Formatted [50]
- Deleted: (2):
- Deleted: Dow, C. F. (2019). *How well does the equal-pres... [51]*
- Deleted: G. ...urand, S. L...., Cornford, G. H.... L., ... [52]
- Deleted: (2):
- Formatted [53]
- Deleted: A. ...evermann (2015), "... A.: Collapse of the W... [54]
- Deleted: (46):
- Formatted [55]
- Deleted: A. F. ...hompson, M. P.... F., Schodlok, H.... P... [56]
- Deleted: (31):
- Formatted [57]
- Deleted: C. X. ...T. Hewitt, G.... X., Aðalgeirsdóttir, S. ... [58]
- Formatted [59]
- Deleted: :

Garbe, J., Albrecht, T., Levermann, A., Donges, J. F., and Winkelmann, R.: The hysteresis of the Antarctic ice sheet, *Nature*, 585, 538-544, 2020.

630 Goelzer, H., Coulon, V., Pattyn, F., De Boer, B., and Van De Wal, R.: Brief communication: On calculating the sea-level contribution in marine ice-sheet models, *The Cryosphere*, 14, 833-840, 2020.

Goldberg, D., Heimbach, P., Joughin, I., and Smith, B.: Committed retreat of Smith, Pope, and Kohler Glaciers over the next 30 years inferred by transient model calibration, *The Cryosphere*, 9, 2429-2446, 2015.

635 Goldberg, D. N.: A variationally derived, depth-integrated approximation to a higher-order glaciological flow model, *Journal of Glaciology*, 57, 157-170, 2011.

Golledge, N. R., Clark, P. U., He, F., Dutton, A., Turney, C., Fogwill, C., Naish, T., Levy, R. H., McKay, R. M., and Lowry, D. P.: Retreat of the Antarctic Ice Sheet during the Last Interglaciation and implications for future change, *Geophysical Research Letters*, 48, e2021GL094513, 2021.

640 Graham, A. G., Wählin, A., Hogan, K. A., Nitsche, F. O., Heywood, K. J., Totten, R. L., Smith, J. A., Hillenbrand, C.-D., Simkins, L. M., and Anderson, J. B.: Rapid retreat of Thwaites Glacier in the pre-satellite era, *Nature Geoscience*, 15, 706-713, 2022.

Greene, C. A., Gardner, A. S., Schlegel, N.-J., and Fraser, A. D.: Antarctic calving loss rivals ice-shelf thinning, *Nature*, 609, 948-953, 2022.

645 Greve, R. and Blatter, H.: Comparison of thermodynamics solvers in the polythermal ice sheet model SICOPOLIS, *Polar Science*, 10, 11-23, 2016.

Gudmundsson, G., Krug, J., Durand, G., Favier, L., and Gagliardini, O.: The stability of grounding lines on retrograde slopes, *The Cryosphere*, 6, 1497-1505, 2012.

Gudmundsson, G. H., Barnes, J. M., Goldberg, D., and Morlighem, M.: Limited impact of Thwaites Ice Shelf on future ice loss from Antarctica, *Geophysical Research Letters*, 50, e2023GL102880, 2023.

650 Gudmundsson, G. H., Paolo, F. S., Adusumilli, S., and Fricker, H. A.: Instantaneous Antarctic ice sheet mass loss driven by thinning ice shelves, *Geophysical Research Letters*, 46, 13903-13909, 2019.

Hellmer, H. H.: Impact of Antarctic ice shelf basal melting on sea ice and deep ocean properties, *Geophysical Research Letters*, 31, 2004.

655 Hill, E. A., Urruty, B., Reese, R., Garbe, J., Gagliardini, O., Durand, G., Gillet-Chaulet, F., Gudmundsson, G. H., Winkelmann, R., and Chekki, M.: The stability of present-day Antarctic grounding lines—Part 1: No indication of marine ice sheet instability in the current geometry, *The Cryosphere*, 17, 3739-3759, 2023.

Hoffman, M. J., Perego, M., Price, S. F., Lipscomb, W. H., Zhang, T., Jacobsen, D., Tezaur, J., Salinger, A. G., Tuminaro, R., and Bertagna, L.: MPAS-Albany Land Ice (MALI): a variable-resolution ice sheet model for Earth system modeling using Voronoi grids, *Geoscientific Model Development*, 11, 3747-3780, 2018.

660 Holland, P. R., Bracegirdle, T. J., Dutrieux, P., Jenkins, A., and Steig, E. J.: West Antarctic ice loss influenced by internal climate variability and anthropogenic forcing, *Nature Geoscience*, 12, 718-724, 2019.

Jacobs, S., Jenkins, A., Giulivi, C., and Dutrieux, P.: Stronger sub-ice shelf ocean circulation undermining the Pine Island Glacier, *Nature Geoscience*, 4, 519-523, 2011a.

665 Jacobs, S. S., Jenkins, A., Giulivi, C. F., and Dutrieux, P.: Stronger ocean circulation and increased melting under Pine Island Glacier ice shelf, *Nature Geoscience*, 4, 519-523, 2011b.

Jenkins, A., Dutrieux, P., Jacobs, S., Steig, E. J., Gudmundsson, G. H., Smith, J., and Heywood, K. J.: Decadal ocean forcing and Antarctic ice sheet response: Lessons from the Amundsen Sea, *Oceanography*, 29, 106-117, 2016.

Joughin, I., Smith, B. E., and Medley, B.: Marine ice sheet collapse potentially under way for the Thwaites Glacier Basin, West Antarctica, *Science*, 344, 735-738, 2014.

670 Joughin, I., Smith, B. E., and Schoof, C. G.: Regularized Coulomb friction laws for ice sheet sliding: Application to Pine Island Glacier, Antarctica, *Geophysical research letters*, 46, 4764-4771, 2019.

Jourdain, N. C., Asay-Davis, X., Hattermann, T., Straneo, F., Seroussi, H., Little, C. M., and Nowicki, S.: A protocol for calculating basal melt rates in the ISMIP6 Antarctic ice sheet projections, *The Cryosphere*, 14, 3111-3134, 2020.

675 Kachuck, S. B., Martin, D. F., Bassis, J. N., and Price, S. F.: Rapid viscoelastic deformation slows marine ice sheet instability at Pine Island Glacier, *Geophysical Research Letters*, 47, e2019GL086446, 2020.

Kazmierczak, E., Gregov, T., Coulon, V., and Pattyn, F.: A fast and unified subglacial hydrological model applied to Thwaites Glacier, Antarctica, *EGU Sphere*, 2024, 1-36, 2024.

Deleted:	T. ...lbrecht, A. ...., Levermann, J. F. ...., Donges (... [60]
Formatted	(... [61]
Deleted:	(7826):
Deleted:	V. ...oulon, F. ...., Pattyn, B. ...., De Boer, B., and (... [62]
Deleted:	(3):
Formatted	(... [63]
Deleted:	. (2011). "...: A variationally derived, depth-integ (... [64]
Formatted	(... [65]
Deleted:	(201):
Deleted:	P. U. ...lark, F. .... U., He, A. ...., Dutton, C. ...., (... [66]
Formatted	(... [67]
Deleted:	(17):
Deleted:	A. S. ...ardner, N.-J. .... S., Schlegel, N.-J., and (... [68]
Deleted:	(7929):
Formatted	(... [69]
Deleted:	H. ...latter (2016). "... H.: Comparison of (... [70]
Formatted	(... [71]
Deleted:	(1):
Deleted:	J. ...rug, G. ...., Durand, L. ...., Favier, L., and O (... [72]
Deleted:	(6):
Formatted	(... [73]
Moved (insertion) [11]	
Deleted:	Gudmundsson, G. H., J. M.
Deleted:	D. .... M., Goldberg, D., and M. ...orlighem (202 (... [74]
Deleted:	(11):
Formatted	(... [75]
Moved up [11]:	Gudmundsson, G. H.,
Deleted:	F. S. ...aolo, F. S. ...., Adusumilli, S., and H. A. ... (... [76]
Deleted:	(23):
Formatted	(... [77]
Deleted:	. (2004). "...: Impact of Antarctic ice shelf basal (... [78]
Formatted	(... [79]
Deleted:	(10)
Deleted:	M. ....Perego, S. F. ...., Price, W. H. ...., F., Lipsco (... [80]
Formatted	(... [81]
Deleted:	(9):
Deleted:	T. J. ...racegirdle, P. .... J., Dutrieux, A. ...., Jenki (... [82]
Formatted	(... [83]
Deleted:	(9):
Deleted:	A. ...enkins, C. ...., Giulivi, C., and P. ...utrieux (... [84]
Formatted	(... [85]
Deleted:	:
Deleted:	A. ...enkins, C. F. ...., Giulivi, C. F., and P. ...utr (... [86]
Formatted	(... [87]
Deleted:	(8):
Deleted:	P. ...utrieux, S. ...., Jacobs, E. J. ...., Steig, G. H. (... [88]
Formatted	(... [89]
Deleted:	(4):
Deleted:	B. E. ...mith, B. E., and B. ...edley (2014). "... B (... [90]
Formatted	(... [91]
Deleted:	(6185):
Deleted:	B. E. ...mith, B. E., and C. G. ...choof (2019). "... (... [92]
Formatted	(... [93]
Deleted:	(9):
Deleted:	X. ...say-Davis, T. ...attermann, F. ...traneo (... [94]



Lambeck, K. and Nakiboglu, S.: Seamount loading and stress in the ocean lithosphere, *Journal of Geophysical Research: Solid Earth*, **85**, 6403-6418, 1980.

1955 Larour, E., Seroussi, H., Morlighem, M., and Rignot, E.: Continental scale, high order, high spatial resolution, ice sheet modeling using the Ice Sheet System Model (ISSM), *Journal of Geophysical Research: Earth Surface*, **117**, 2012.

Leguy, G., Asay-Davis, X., and Lipscomb, W.: Parameterization of basal friction near grounding lines in a one-dimensional ice sheet model, *The Cryosphere*, **8**, 1239-1259, 2014.

1960 Leguy, G. R., Lipscomb, W. H., and Asay-Davis, X. S.: Marine ice sheet experiments with the Community Ice Sheet Model, *The Cryosphere*, **15**, 3229-3253, 2021.

Lhermitte, S., Sun, S., Shuman, C., Wouters, B., Pattyn, F., Wuite, J., Berthier, E., and Nagler, T.: Damage accelerates ice shelf instability and mass loss in Amundsen Sea Embayment, *Proceedings of the National Academy of Sciences*, **117**, 24735-24741, 2020.

Lipscomb, W. H., Leguy, G. R., Jourdain, N. C., Asay-Davis, X., Seroussi, H., and Nowicki, S.: ISMIP6-based projections of ocean-forced Antarctic Ice Sheet evolution using the Community Ice Sheet Model, *The Cryosphere*, **15**, 633-661, 2021.

1965 Lipscomb, W. H., Price, S. F., Hoffman, M. J., Leguy, G. R., Bennett, A. R., Bradley, S. L., Evans, K. J., Fyke, J. G., Kennedy, J. H., and Perego, M.: Description and evaluation of the community ice sheet model (CISM) v2. 1, *Geoscientific Model Development*, **12**, 387-424, 2019.

Milillo, P., Rignot, E., Rizzoli, P., Scheuchl, B., Mouginito, J., Bueso-Bello, J., and Prats-Iraola, P.: Heterogeneous retreat and ice melt of Thwaites Glacier, West Antarctica, *Science advances*, **5**, eaau3433, 2019.

1970 Morlighem, M., Rignot, E., Binder, T., Blankenship, D., Drews, R., Eagles, G., Eisen, O., Ferraccioli, F., Forsberg, R., and Fretwell, P.: Deep glacial troughs and stabilizing ridges unveiled beneath the margins of the Antarctic ice sheet, *Nature Geoscience*, **13**, 132-137, 2020.

Naughten, K. A., Holland, P. R., and De Rydt, J.: Unavoidable future increase in West Antarctic ice-shelf melting over the twenty-first century, *Nature Climate Change*, [10.1038/s41558-023-01818-x](https://doi.org/10.1038/s41558-023-01818-x), 2023.

1975 Payne, A. J., Nowicki, S., Abe-Ouchi, A., Agosta, C., Alexander, P., Albrecht, T., Asay-Davis, X., Aschwanden, A., Barthel, A., and Bracegirdle, T. J.: Future sea level change under coupled model intercomparison project phase 5 and phase 6 scenarios from the Greenland and Antarctic ice sheets, *Geophysical Research Letters*, **48**, e2020GL091741, 2021.

Pollard, D. and DeConto, R.: Description of a hybrid ice sheet-shelf model, and application to Antarctica, *Geoscientific Model Development*, **5**, 1273-1295, 2012.

1980 Quiquet, A., Dumas, C., Ritz, C., Peyaud, V., and Roche, D. M.: The GRISLI ice sheet model (version 2.0): calibration and validation for multi-millennial changes of the Antarctic ice sheet, *Geoscientific Model Development*, **11**, 5003-5025, 2018.

Reese, R., Garbe, J., Hill, E. A., Urruty, B., Naughten, K. A., Gagliardini, O., Durand, G., Gillet-Chaulet, F., Gudmundsson, G. H., and Chandler, D.: The stability of present-day Antarctic grounding lines—Part 2: Onset of irreversible retreat of Amundsen Sea glaciers under current climate on centennial timescales cannot be excluded, *The Cryosphere*, **17**, 3761-3783, 2023.

1985 Rémy, F. and Legresy, B.: Subglacial hydrological networks in Antarctica and their impact on ice flow, *Annals of Glaciology*, **39**, 67-72, 2004.

Rignot, E., Jacobs, S., Mouginito, J., and Scheuchl, B.: Ice-shelf melting around Antarctica, *Science*, **341**, 266-270, 2013.

1990 Rignot, E., Mouginito, J., Morlighem, M., Seroussi, H., and Scheuchl, B.: Widespread, rapid grounding line retreat of Pine Island, Thwaites, Smith, and Kohler glaciers, West Antarctica, from 1992 to 2011, *Geophysical Research Letters*, **41**, 3502-3509, 2014.

Rignot, E., Mouginito, J., Scheuchl, B., Van Den Broeke, M., Van Wessem, M. J., and Morlighem, M.: Four decades of Antarctic Ice Sheet mass balance from 1979–2017, *Proceedings of the National Academy of Sciences*, **116**, 1095-1103, 2019.

1995 Robel, A. A., Seroussi, H., and Roe, G. H.: Marine ice sheet instability amplifies and skews uncertainty in projections of future sea-level rise, *Proceedings of the National Academy of Sciences*, **116**, 14887-14892, 2019.

Robinson, A., Goldberg, D., and Lipscomb, W. H.: A comparison of the stability and performance of depth-integrated ice-dynamics solvers, *The Cryosphere*, **16**, 689-709, 2022.

2000 Rosier, S. H., Gudmundsson, G. H., Jenkins, A., and Naughten, K. A.: Calibrated sea level contribution from the Amundsen Sea sector, West Antarctica, under RCP8.5 and Paris 2C scenarios [preprint], *EGUosphere*, 2024.

Rosier, S. H., Reese, R., Donges, J. F., De Rydt, J., Gudmundsson, G. H., and Winkelmann, R.: The tipping points and early warning indicators for Pine Island Glacier, West Antarctica, *The Cryosphere*, **15**, 1501-1516, 2021.

Deleted: S. ...akiboglu (1980). "... S.: Seamount loading (... [98]

Formatted (... [99]

Deleted: (B11):

Deleted: H. ...eroussi, M....., Morlighem, M., and E...R (... [100]

Formatted (... [101]

Deleted: (F1)

Deleted: X. ...say-Davis, X., and W. ...ipscomb (2014). (... [102]

Formatted (... [103]

Deleted: (4):

Deleted: W. H. ...ipscomb, W. H., and X. S. ...say-Davis (... [104]

Deleted: (7):

Formatted (... [105]

Deleted: S. ...un, C....., Shuman, B....., Wouters, F..... (... [106]

Deleted: (40):

Formatted (... [107]

Deleted: G. R. ...eguy, N. C..... R., Jourdain, X..... C., A (... [108]

Formatted (... [109]

Deleted: (2):

Deleted: S. F. ...rice, M. J..... F., Hoffman, G. R..... J., I (... [110]

Formatted (... [111]

Deleted: (1):

Deleted: Martos, Y. M., M. Catalán, T. A. Jordan, A. Gol (... [112]

Deleted: (1):

Formatted (... [113]

Deleted: E. ...ignot, T....., Binder, D....., Blankenship, R (... [114]

Formatted (... [115]

Deleted: (2):

Deleted: P. R. ...olland, P. R., and J. ...e Rydt (2023). "... [116]

Formatted (... [117]

Deleted: Naughten, K. A., P. R. Holland, P. Dutrieux, S. (... [118]

Deleted: (16):

Formatted (... [119]

Deleted: R. ...eConto (2012). "... R.: Description of a hy (... [120]

Formatted (... [121]

Deleted: (5):

Deleted: C. ...umas, C....., Ritz, V....., Peyaud, V., and D (... [122]

Deleted: (12):

Formatted (... [123]

Deleted: J. ...arbe, E. A....., Hill, B..... A., Urruty, K. A. (... [124]

Deleted: (9):

Formatted (... [125]

Deleted: B. ...egresy (2004). "... B.: Subglacial hydrolog (... [126]

Formatted (... [127]

Deleted: :

Deleted: S. ...acobs, J....., Mouginito, J., and B. ...cheuch (... [128]

Deleted: (6143):

Formatted (... [129]

Deleted: J. ...ouginito, M....., Morlighem, H....., Seroussi (... [130]

Deleted: (10):

Formatted (... [131]

Deleted: J. ...ouginito, B....., Scheuchl, M....., Van Den (... [132]

Deleted: (4):

Formatted (... [133]

Deleted: D. ...oldberg, D., and W. H. ...ipscomb (2022). (... [134]

Deleted: (2):



Schoof, C.: Ice sheet grounding line dynamics: Steady states, stability, and hysteresis, *Journal of Geophysical Research: Earth Surface*, **112**, 2007.

Schoof, C.: Marine ice sheet stability, *Journal of Fluid Mechanics*, **698**, 62-72, 2012.

Seroussi, H., Nowicki, S., Payne, A. J., Goelzer, H., Lipscomb, W. H., Abe-Ouchi, A., Agosta, C., Albrecht, T., Asay-Davis, X., and Barthel, A.: ISMIP6 Antarctica: a multi-model ensemble of the Antarctic ice sheet evolution over the 21st century, *The Cryosphere*, **14**, 3033-3070, 2020.

Seroussi, H., Pelle, T., Lipscomb, W. H., Abe-Ouchi, A., Albrecht, T., Alvarez-Solas, J., Asay-Davis, X., Barre, J. B., Berends, C. J., and Bernales, J.: Evolution of the Antarctic Ice Sheet over the next three centuries from an JSMIP6 model ensemble, *Earth's Future*, **12**, e2024EF004561, 2024.

Silvano, A., Holland, P. R., Naughten, K. A., Dragomir, O., Dutrieux, P., Jenkins, A., Si, Y., Stewart, A. L., Peña Molino, B., and Janzing, G. W.: Baroclinic Ocean Response to Climate Forcing Regulates Decadal Variability of Ice-Shelf Melting in the Amundsen Sea, *Geophysical Research Letters*, **49**, e2022GL100646, 2022.

Smith, B., Fricker, H. A., Gardner, A. S., Medley, B., Nilsson, J., Paolo, F. S., Holschuh, N., Adusumilli, S., Brunt, K., and Csatho, B.: Pervasive ice sheet mass loss reflects competing ocean and atmosphere processes, *Science*, **368**, 1239-1242, 2020.

Swart, N. C., Martin, T., Beadling, R., Chen, J.-J., Danek, C., England, M. H., Farneti, R., Griffies, S. M., Hattermann, T., and Hauck, J.: The Southern Ocean Freshwater Input from Antarctica (SOFIA) Initiative: scientific objectives and experimental design, *Geoscientific Model Development*, **16**, 7289-7309, 2023.

Thoma, M., Jenkins, A., Holland, D., and Jacobs, S.: Modelling circumpolar deep water intrusions on the Amundsen Sea continental shelf, Antarctica, *Geophysical Research Letters*, **35**, 2008.

Van Calcar, C. J., Van De Wal, R. S., Blank, B., De Boer, B., and Van Der Wal, W.: Simulation of a fully coupled 3D glacial isostatic adjustment-ice sheet model for the Antarctic ice sheet over a glacial cycle, *Geoscientific Model Development*, **16**, 5473-5492, 2023.

van de Wal, R. S., Nicholls, R. J., Behar, D., McInnes, K., Stammer, D., Lowe, J. A., Church, J. A., DeConto, R., Fettweis, X., and Goelzer, H.: A High-End Estimate of Sea Level Rise for Practitioners, *Earth's future*, **10**, e2022EF002751, 2022.

van der Wel, N., Christoffersen, P., and Bougamont, M.: The influence of subglacial hydrology on the flow of Kamb Ice Stream, West Antarctica, *Journal of Geophysical Research: Earth Surface*, **118**, 97-110, 2013.

Van Wessem, J. M., Van De Berg, W. J., Noël, B. P., Van Meijgaard, E., Amory, C., Birnbaum, G., Jakobs, C. L., Krüger, K., Lenaerts, J. T., and Lhermitte, S.: Modelling the climate and surface mass balance of polar ice sheets using RACMO2-Part 2: Antarctica (1979–2016), *The Cryosphere*, **12**, 1479-1498, 2018.

Williams, G., Herraiz-Borreguero, L., Roquet, F., Tamura, T., Ohshima, K., Fukamachi, Y., Fraser, A., Gao, L., Chen, H., and McMahon, C.: The suppression of Antarctic bottom water formation by melting ice shelves in Prydz Bay, *Nature communications*, **7**, 12577, 2016.

Wilner, J. A., Morlighem, M., and Cheng, G.: Evaluation of four calving laws for Antarctic ice shelves, *The Cryosphere Discussions*, **2023**, 1-19, 2023.

Winkelmann, R., Martin, M. A., Haseloff, M., Albrecht, T., Bueler, E., Khroulev, C., and Levermann, A.: The Potsdam parallel ice sheet model (PISM-PIK)-Part 1: Model description, *The Cryosphere*, **5**, 715-726, 2011.

Yu, H., Rignot, E., Seroussi, H., Morlighem, M., and Choi, Y.: Impact of iceberg calving on the retreat of Thwaites Glacier, West Antarctica over the next century with different calving laws and ocean thermal forcing, *Geophysical Research Letters*, **46**, 14539-14547, 2019.

Zoet, L. K. and Iverson, N. R.: A slip law for glaciers on deformable beds, *Science*, **368**, 76-78, 2020.

Zwally, H. J., Li, J., Robbins, J. W., Saba, J. L., Yi, D., and Brenner, A. C.: Mass gains of the Antarctic ice sheet exceed losses, *Journal of Glaciology*, **61**, 1019-1036, 2015.

- Deleted: . (2012). "Marine ice...: Ice sheet grounding lin... [138]
- Deleted: :
- Formatted [139]
- Moved (insertion) [12]
- Deleted: Schoof, C. and I. Hewitt (2013). "Ice-sheet dyna... [140]
- Deleted: A. J....., Payne, H..... J., Goelzer, W. ...., Lip... [141]
- Deleted: (9):
- Formatted [142]
- Moved up [12]: Seroussi, H.,
- Deleted: S. Nowicki, E. Simon, A.....eroussi, H., Pelle, T (... [143]
- Deleted: P. R. ...olland, K. A..... R., Naughten, O..... A. (... [144]
- Deleted: (24):
- Formatted [145]
- Deleted: H. A. ...ricker, H. A. S....., Gardner, B..... S., M... [146]
- Deleted: (6496):
- Formatted [147]
- Deleted: Sun, S., F. Pattyn, E. G. Simon, T. Albrecht, S. (... [148]
- Deleted: (24):
- Formatted [149]
- Deleted: A. ...enkins, D....., Holland, D., and S. ...acobs (... [150]
- Formatted [151]
- Deleted: (18)
- Deleted: R. J. ...icholls, D..... J., Behar, K....., McInnes, (... [152]
- Deleted: (11):
- Formatted [153]
- Deleted: P. ...hristoffersen, P., and M. ...ougamont (201... [154]
- Deleted: (1):
- Formatted [155]
- Deleted: W. J. ...an De Berg, B. P..... J., Noël, E..... P., (... [156]
- Deleted: (4):
- Formatted [157]
- Deleted: M....Morlighem, M., and G. ...heng (2023). "... [158]
- Formatted [159]
- Deleted: : 1-19
- Deleted: M. A. ...artin, M. A., Haseloff, T....., Albrecht, (... [160]
- Deleted: (3):
- Formatted [161]
- Deleted: E. ...ignot, H....., Seroussi, M....., Morlighem, (... [162]
- Formatted [163]
- Deleted: (24):
- Deleted: N. R. ...iverson (2020). "... N. R.: A slip law for (... [164]
- Deleted: (6486):
- Formatted [165]